Chinese Journal of Chemical Engineering 58 (2023) 53–68

Contents lists available at ScienceDirect

Chinese Journal of Chemical Engineering

journal homepage: www.elsevier.com/locate/CJChE

Full Length Article

Thermogravimetric analysis and kinetic modeling of the co-pyrolysis of a bituminous coal and poplar wood

Wei Wang [1,2], Romain Lemaire [1,*], Ammar Bensakhria [2], Denis Luart [3]

[1] Department of Mechanical Engineering, École de technologie supérieure, Montreal, Quebec H3C 1K3, Canada
[2] Université de Technologie de Compiègne, Centre de recherche de Royallieu, EA 4297-TIMR, BP20529, 60205 Compiègne, France
[3] École Supérieure de Chimie Organique et Minérale, 1 Rue du Réseau Jean-Marie Buckmaster, 60200 Compiègne, France

ARTICLE INFO

Article history:
Received 24 June 2022
Received in revised form 1 October 2022
Accepted 12 October 2022
Available online 11 November 2022

Keywords:
Co-pyrolysis
Coal
Wood
Kinetics
Synergistic effects

ABSTRACT

The co-pyrolysis of coal and biomass has proven to be a promising route to produce liquid and gaseous fuels as well as specific value-added chemicals while contributing to mitigating CO_2 emissions. The interactions between the co-processed feedstocks, however, need to be elucidated to support the development of such a thermochemical conversion process. In this context, the present work covers the kinetic analysis of the co-pyrolysis of a bituminous coal with poplar wood. In this research, biomass was blended with coal at two different mass ratios (10% (mass) and 20% (mass)). Thermogravimetric analyses were carried out with pure and blended samples at four heating rates (5, 10, 15 and 30 °C·min^{-1}). A direct comparison of experimental and theoretical results (based on a simple additivity rule) failed to yield a clear-cut conclusion regarding the existence of synergistic effects. Kinetic analyses have therefore been achieved using two model-free methods (the Ozawa–Flynn–Wall and Kissinger–Akahira–Sunose models) to estimate the rate constant parameters related to the pyrolysis process. A significant decrease of the activation energy has thus been observed when adding wood to coal (activation energies associated with the blend containing 20% (mass) of biomass being even lower than those estimated for pure wood at low conversion degrees). This trend was attributed to the possible presence of synergies whose related mechanisms are discussed. The rate constant parameters derived by means of the two tested models were finally used to simulate the evolution of the conversion degree of each sample as a function of the temperature, thus leading to a satisfying agreement between measured and simulated data.

1. Introduction

Coal is one of the most used energy resources in various countries, including China and India. Despite the high CO_2 and pollutant emissions resulting from its use, coal will still play a key role in the electricity and heat production sectors in future decades. Nevertheless, given the increasing concerns about climate change, coal-based power plants will have to face ever more stringent regulations aimed at limiting CO_2 emissions. In this context, biomass-derived fuels represent an alternative option to gradually reduce the consumption of fossil resources since the addition of biomass can drastically decrease net CO_2 emissions. The use of such a renewable fuel may potentially extend the operating life of existing coal-based power plants with reasonable upgrading costs (especially when biomass is mixed with coal at relatively low blending ratios as investigated herein). Carbon-neutral biomass with a lower sulfur and nitrogen content is thus gaining increasing attention from researchers and industry. Nevertheless, due to its seasonal availability, high heterogeneity, low heating value and low density, it is difficult to steadily and continuously use biomass as the sole feedstock for power plant applications [1]. Co-combustion or co-gasification of coal with biomass are possible routes to address such problems [2].

Pyrolysis is the first, and therefore especially important step, in co-combustion and co-gasification processes. It thus needs to be thoroughly characterized in terms of kinetic mechanisms to properly design and optimize the functioning of industrial scale boilers, power plants and pyrolysis facilities. This need is all the more crucial when considering the growing attention paid to thermochemical conversion processes involving biomass-based energy carriers in the production of fuels and chemicals [3,4]. Compared to biochemical routes (*e.g.*, digestion and fermentation), biomass

* Corresponding author at: École de technologie supérieure, Montreal, Department of Mechanical Engineering, Quebec H3C 1K3, Canada.
E-mail address: romain.lemaire@etsmtl.ca (R. Lemaire).

https://doi.org/10.1016/j.cjche.2022.10.015
1004-9541/

pyrolysis represents a promising platform for producing char, liquid and gaseous fuels, as well as specific value-added chemicals. Being much more rapid than biochemical processes [5], pyrolysis, which is conducted at relatively moderate temperatures [6], also presents economic advantages over other pathways [7,8]. Blending biomass with fossil fuels such as coal, moreover, allows reducing the feedstock moisture content while improving its grindability. Besides, the alkali and alkaline earth metals present in biomass are likely to play an important catalytic role in devolatilization and cracking reactions, thus affecting the thermal reactivity of the co-processed fuels as well as the properties of the generated products as reviewed in [3]. For instance, co-pyrolyzing coal with biomass can increase the yield of emitted volatiles and thus enhance the overall efficiency of the conversion process. Increasing the biomass blending ratio can, moreover, increase the liquid and gas yields at the expense of the char one. Besides, the higher H/C ratio of biomass is prone to inhibit the yield of heavy oil produced during co-pyrolysis, while the alkali and alkaline earth metals which are present in lignocellulosic biomass are likely to increase the reactivity of obtained char (see [3] and references therein).

All these observations explain why co-pyrolysis of coal with biomass has been investigated extensively in the literature since the 1960s, especially since synergistic effects have been evidenced by some researchers. The term synergy implies that the interaction of coal and biomass when these feedstocks are combined induces a greater positive effect (in terms of energy savings, product quality or emission reduction) than does the simple sum of these individual components [9]. Synergistic effects are more evident when biomass is combined with low-rank coals since the latter yield more volatiles and contain larger pores, which promote devolatilization reactions [10,11]. Specifically, synergistic effects can be related to a decrease of the activation energy [2,10,12], a reduction of the pyrolysis temperatures [2,10,13] or an enhancement of the yields of volatile and gaseous species [1,10,12–16]. Notwithstanding the large number of investigations that have been led in recent years, many aspects of synergistic effects have still not been fully elucidated due to the large variety of coal and biomass that are commonly used [1]. For instance, it is still not clear whether or not an enhancement of mass loss does exist since some works do not show any remarkable interactions between coal and biomass [17–19], notably as far as increases in the yields of volatile species are concerned [20]. Furthermore, some researchers have also drawn somewhat contrasting conclusions regarding the distribution of pyrolytic products when adding biomass to coal. It has been demonstrated that the higher oxygen and hydrogen contents of biomass leads to increased yields of some species, such as CO [15,21,22], H_2 [15,22], CH_4 [15,22], acetic acid [14], aliphatic hydrocarbons [22], and phenols [13]. For instance, Li *et al.* [23] pointed out that the co-pyrolysis of rice straw and bituminous coal could promote the yields of CO, CO_2, H_2 and phenolics, while inhibiting the production of oxygenated compounds. They inferred that the synergistic effect originates from secondary reactions involving volatile tar, but not from the interactions between solid chars. Conversely, some researchers reported opposite trends concerning the synergistic effects on the pyrolysis product distribution. Soncini *et al.* investigated the evolution of light gases during the fast co-pyrolysis of pine wood and two types of coal, with heating rates reaching up to 1000 $°C·s^{-1}$ [11]. In general, an increase in tar production at the expense of light gases was observed. This trend can be related to the stabilization of the large radical structures produced during the early stages of coal pyrolysis by hydrogen coming from the rapid decomposition of biomass, thus inhibiting secondary gasification reactions [11]. In a work by Ma *et al.* on the co-pyrolysis of cow manure and bituminous coal, the production of H_2 was shown to be inhibited by the addition of biomass [21]. According to these authors, the high oxygen content in cow manure would combine with reactive hydrogen radicals to form H_2O [21]. Based on these experimental observations, it can be seen that the synergistic effects are impacted by many factors, such as the temperature, the heating rate, the biomass type, the coal rank, as well as the blending ratio. It is thus difficult to draw general conclusions on the matter [1,9,13,22]. Furthermore, and as far as the last operating factor is concerned (*i.e.*, the blending ratio), it is noteworthy that most of the studies undertaken to evidence and/or elucidate synergistic effects have been conducted using biomass amounts exceeding 25% (mass) (see the above-cited works as well as [3] and references therein). As far as kinetic analyses are concerned, few works have selected blending ratios lower than 20% (mass), although [15] demonstrated that wood contents below 16% were preferable for a better use of poplar-coal blends, for instance. Further studies investigating the possible synergies at play when co-pyrolyzing coal with biomass added in relatively low quantities (*i.e.*, below 20% (mass)) are therefore required, especially when considering the concerns which may stem from the use of high mixing ratios in terms of biomass supply limitations and retrofitting costs of coal-based industrial scale processes [24].

In an attempt to analyze the mechanisms underlying the synergistic effects occurring during the co-pyrolysis of two feedstocks (a woody biomass added to a high volatile bituminous coal at 10% (mass) and 20% (mass)), the present study covers the kinetic analysis of a dataset experimentally acquired using thermogravimetric analysis (TGA). Various works conducted using such a widely implemented non-isothermal method have reported more or less pronounced decreases of the activation energy (E_a) during co-pyrolysis. Decreases of E_a actually tend to indicate that less external energy is needed to overcome the energy barrier allowing pyrolysis to take place, hence indicating possible synergistic effects. Here again, this phenomenon, however, largely depends on the coal rank [1,10], the temperature range [1,10] and the blending ratio [1,10,12,15,25], thus prompting the need for more investigations [3]. As for existing and currently used kinetic models, one can cite the widely used model-fitting and model-free methods [26], the distributed activation energy models (DAEM) [27], the lumped kinetic [28–30] or the chemical percolation devolatilization models [31,32]. These can be roughly classified into two categories, depending on whether they aim at simulating the mass loss rate of the fuel or the distribution of the pyrolytic products [4]. In the context of TGA-based kinetic analyses, model-fitting and model-free methods have been extensively applied with the view to assessing E_a values [4]. The Coats-Redfern model is currently the most commonly implemented model-fitting approach used to study the kinetics of coal and biomass pyrolysis [14,33–37]. Although it generally provides good data fittings, the kinetic parameters obtained from the Coats-Redfern model might not be reliable and consistent as they depend on an a priori assumption made on the selected reaction model. To tackle this issue, model-free methods represent a more accurate route to infer E_a, which can be directly calculated without the need for any initial assumption regarding the reaction model [4,38]. As far as the selection of a proper reaction model is concerned, two possible approaches have been summarized in the review by Wang *et al.* [4]. The first one concerns the use of the master plot method which allows selecting the most suitable reaction model by comparing experimental curves to some pre-established theoretical ones (provided that the studied phenomenon corresponds to a single-step process) [39–42]. The second solution relies on the comparison of the values of the activation energy derived from model-free and model-fitting methods. Assuming that the model-free method allows assessing more accurate activation energies, these E_a values should therefore be considered in the model-fitting procedure in order to select an appropriate reaction model

allowing to derive similar activation energies [42–45]. Apart from the two above-mentioned routes, the adapted reaction models can also be selected by directly modeling the mass loss curves based on Arrhenius-type equations in order to obtain simulated results merging on a single curve with experimentally monitored ones. Even though the kinetic models discussed above have been largely used to analyze the pyrolysis of coal and/or biomass, a few works still try to reproduce measured evolutions of the conversion degree of the fuels as a function of the temperature, using the so-assessed kinetic parameters. Exceptions include the works by [19,46–48] who respectively considered Coats-Redfern [19,46] and model-free [47,48] methods. Complementary modeling analyses focusing on the co-pyrolysis of coal and wood would, therefore, be beneficial.

Based on the gaps identified above, 2 model-free methods (the Ozawa–Flynn–Wall (OFW) [38,49] and Kissinger–Akahira–Sunose (KAS) [50,51] models) were selected to investigate the possible synergistic effects encompassing the co-pyrolysis of a high volatile bituminous coal with a typical lignocellulosic biomass. Poplar wood was considered for that purpose due to its capacity to be a major feedstock for the bio-based-economy, which covers green chemicals and energy [52]. Widely available and distributed in many countries, including Canada and China, poplar, when grown using a short rotation coppice system, presents numerous advantages in terms of adaptability, long annual growth period, fast growth rate, as well as ecological interest and comparatively low biomass production costs [52,53]. Rich in lignocellulose, the pyrolysis of poplar wood is prone to induce a high bio-oil yield, thus explaining why the thermal decomposition of this feedstock (notably when used in blends to improve the quality of obtained products) has been increasingly studied in recent years (see [15,54] as examples). 16 different reaction models were considered herein to perform the proposed modeling study. Calculations were then made to simulate the conversion degree profiles of each sample with the two above-mentioned methods. Finally, the obtained results were analyzed to better understand the relative impact of blending coal with wood on pyrolysis kinetics.

2. Methodology

2.1. Feedstocks

A high volatile bituminous coal from La Loma (similar to the one previously used in [55–57]) was selected to be blended with poplar wood. For simplicity purposes, these feedstocks will be referred to as 'coal' and 'wood'. Their proximate and ultimate analyses are provided in Table 1. Each fuel was ground in an industrial grinder and sieved into a size fraction of 40–125 μm. Wood was then blended with coal at mass fractions of 10% and 20% to obtain 'coal + 10% wood' and 'coal + 20% wood' samples. These blends were thoroughly mixed and homogenized before analysis. All samples (2 pure feedstocks and 2 blends) were dried in an oven with a constant temperature of 105 °C for 24 h to get rid of excess moisture content. The samples were then stored in a desiccator to prevent moisture absorption from the atmosphere before being analyzed in the thermogravimetric analyzer.

2.2. Experimental approach

Pyrolysis experiments were carried out using a Setaram SETSYS Evolution thermogravimetric analyzer at four constant heating rates (5, 10, 15 and 30 °C·min^{-1}) from room temperature up to 950 °C. All the TGA tests were repeated 3 times for each operating condition. All the calculations presented in the following are thus based on averaged mass loss profiles. A mean sample mass of 10 mg was systematically used. Besides, a constant 100 ml·min^{-1} flow of helium was sent to the thermogravimeter during all the tests to eliminate air and continuously ensure an inert environment. The pyrolysis temperature was first held at 105 °C for 20 min to allow a complete removal of free water. Following [58,59], only the section below 700 °C (which represents the main part of the mass loss process) was taken into account for the calculations presented hereafter, especially due to the possible measurement noise recorded at the highest temperatures. Finally, the conversion degree α at any given time t was calculated from the initial (i) and final (f) residual mass (noted TG and expressed in % (mass)) in order to estimate the reaction progression based on Eq. (1):

$$\alpha = \frac{TG_i - TG_t}{TG_i - TG_f} \tag{1}$$

To that end, the measurement point corresponding to a temperature of 106 °C was defined as the initial time and related to a 0% conversion degree, while the final point, which corresponds to a temperature of 700 °C, was associated with a 100% conversion degree.

2.3. Modeling approach

2.3.1. Kinetic theory

Three rate constant parameters, namely, A (s^{-1}, the pre-exponential factor), E_a (kJ·mol^{-1}, the activation energy) and $f_{(\alpha)}$ (the differential reaction model (see Table 2)), are required with a view to simulating and/or predicting mass loss curves [60] based on Eq. (2):

$$\frac{d\alpha}{dt} = k_{(T)} f_{(\alpha)} = A\exp\left(-\frac{E_a}{RT}\right) f_{(\alpha)} \tag{2}$$

where t (s) is the time, T (K) is the temperature, and R is the universal gas constant whose value is 8.314 J·mol^{-1}·K^{-1}.

When a constant heating rate β is implemented, as is the case during the TGA measurements conducted herein, the variation of α can be represented as a function of T as per in Eq. (3):

$$\frac{d\alpha}{dT} = \frac{A}{\beta}\exp\left(-\frac{E_a}{RT}\right) f_{(\alpha)} \tag{3}$$

In most cases, the reaction rate is very weak for temperatures lower than T_0 (*i.e.*, the value taken by T at t = 0). Consequently, the related integral term can be neglected [38]. By integrating both

Table 1
Proximate and ultimate analyses of wood and coal samples

Sample	Proximate analysis		Ultimate analysis				
	Volatiles(db)/% (mass)	Ash(db)/% (mass)	C(db)/% (mass)	H(db)/% (mass)	O(db[①])/% (mass)	N(db)/% (mass)	S(db)/% (mass)
Wood	81.6	1.8	49.20	5.79	43.00	<0.30	0.04
Coal	37.0	4.5	77.00	4.70	12.16	1.18	0.48

Note: db–dry basis; [①]Calculated by difference.

Table 2
Summary of some commonly used reaction models

Reaction model	Code	Differential form $f_{(\alpha)}$	Integral form $g_{(\alpha)}$
Order-based	Mampel first-order (F1)	$(1-\alpha)^1$	$-\ln(1-\alpha)$
	*n*th-order (Fn)	$(1-\alpha)^n$	$[(1-\alpha)^{-(n-1)}-1]/(n-1)$
Diffusion	2-D diffusion (D2)	$[-\ln(1-\alpha)]^{-1}$	$(1-\alpha)\ln(1-\alpha)+\alpha$
	3-D diffusion Jander (D3)	$3/2(1-\alpha)^{2/3}[1-(1-\alpha)^{1/3}]^{-1}$	$[1-(1-\alpha)^{1/3}]^2$
Geometrical contraction	Contracting cylinder (R2)	$2(1-\alpha)^{1/2}$	$1-(1-\alpha)^{1/2}$
	Contracting sphere (R3)	$3(1-\alpha)^{2/3}$	$1-(1-\alpha)^{1/3}$
Nucleation	Avrami-Erofeev (A2)	$2(1-\alpha)[-\ln(1-\alpha)]^{1/2}$	$[-\ln(1-\alpha)]^{1/2}$
	Avrami-Erofeev (A3)	$3(1-\alpha)[-\ln(1-\alpha)]^{2/3}$	$[-\ln(1-\alpha)]^{1/3}$
	Avrami-Erofeev (A4)	$4(1-\alpha)[-\ln(1-\alpha)]^{3/4}$	$[-\ln(1-\alpha)]^{1/4}$
Power law	2-Power law (P2)	$2\alpha^{1/2}$	$\alpha^{1/2}$
	3-Power law (P3)	$3\alpha^{2/3}$	$\alpha^{1/3}$
	4-Power law (P4)	$4\alpha^{3/4}$	$\alpha^{1/4}$

sides of Eq. (3), and assuming the initial temperature and initial conversion degree to be zero, the integral form of the reaction model $g_{(\alpha)}$ can be expressed as follows:

$$g_{(\alpha)}=\int_0^{\alpha}\frac{\mathrm{d}\alpha}{f_{(\alpha)}}=\frac{A}{\beta}\int_{T_0}^{\mathrm{T}}\exp\left(-\frac{E_\mathrm{a}}{RT}\right)\mathrm{d}T\cong\frac{A}{\beta}\int_0^{\mathrm{T}}\exp\left(-\frac{E_\mathrm{a}}{RT}\right)\mathrm{d}T \tag{4}$$

The term on the right-hand side of Eq. (4) corresponds to an exponential integral which has no exact solution (in closed form). An algebraic approximation of this term must therefore be used to enable the calculation [61,62]. By replacing dT by du in the integral (with $u=E_\mathrm{a}/RT$), it is possible to convert the right-hand term of Eq. (4) in the form:

$$g_{(\alpha)}=\frac{A}{\beta}\int_0^{\mathrm{T}}\exp\left(-\frac{E_\mathrm{a}}{RT}\right)\mathrm{d}T=\frac{A}{\beta}\int_{\infty}^{u}(-\mathrm{e}^{-u}\frac{E_\mathrm{a}}{Ru^2})\mathrm{d}u=\frac{AE_\mathrm{a}}{\beta R}\int_u^{+\infty}(\frac{\mathrm{e}^{-u}}{u^2})\mathrm{d}u=\frac{AE_\mathrm{a}}{\beta R}p(u) \tag{5}$$

such that:

$$\ln\left[g_{(\alpha)}\right]=\ln(\frac{AE_\mathrm{a}}{\beta R})+\ln[p(u)] \tag{6}$$

where $p(u)$ is an exponential integral that does not have an analytical solution. Based on Doyle's assumption, one can convert the function $p(u)$ into a series (see Eq. (7)) leading to the expressions of the OFW and KAS models detailed in Section 2.3.2.

$$p(u)=\int_u^{+\infty}\left(\frac{\mathrm{e}^{-u}}{u^2}\right)\mathrm{d}u=\frac{\mathrm{e}^{-u}}{u^2}(1-\frac{2!}{u}+\frac{3!}{u^2}-\frac{4!}{u^3}+\cdots) \tag{7}$$

2.3.2. Model free methods

Two of the most commonly used model-free methods (namely the Ozawa–Flynn–Wall (OFW) [38,49] and Kissinger–Akahira–Sunose (KAS) [50,51] models) have been considered. The theoretical principle underlying these so-called "isoconversional" modeling approaches is summarized in Sections 2.3.2.1 and 2.3.2.2, respectively.

2.3.2.1. OFW isoconversional model. By considering the first two terms of Eq. (7), the expression of $p(u)$ can be simplified as follows:

$$\ln[p(u)]=\ln\left[\frac{\mathrm{e}^{-u}}{u^2}\left(1-\frac{2!}{u}\right)\right]=-u+\ln(u-2)-3\ln(u) \tag{8}$$

Based on the typical temperature range encountered during pyrolysis, u falls approximately between 20 and 60, such that $-1\le(u-40)/20\le1$. By assuming that $v=(u-40)/20$, one obtains $u=20v+40$, hence leading Eq. (8) to be reformulated in the form:

$$\ln[p(u)]=-u+\ln(u-2)-3\ln(u)=-u-3\ln40+\ln38+\ln\left(1+\frac{10}{19}v\right)-3\ln(1+\frac{1}{2}v) \tag{9}$$

The term $\ln[p(u)]$ can then be approximately written as a first-order function of u (*i.e.*,

$\ln[p(u)]\cong-5.331-1.052u$ or $\lg[p(u)]\cong-2.315-0.4567u$). For a given conversion degree α, $\ln[g(\alpha)]$ is constant and the term $\ln(AE_\mathrm{a}/\beta R)+\ln[p(u)]$ also remains constant (see Eq. (6)). Consequently, at different heating rates β_i and temperatures T_i , one can derive the following equalities:

$$\ln\left[\frac{A_1E_{\mathrm{a},1}}{\beta_1R}\right]-5.331-1.052\frac{E_{\mathrm{a},1}}{RT_1}=\ln\left[\frac{\mathrm{A}_2E_{\mathrm{a},2}}{\beta_2R}\right]-5.331-1.052\frac{E_{\mathrm{a},2}}{RT_2}=\cdots \tag{10}$$

By plotting the evolution of $\ln(\beta)$ as a function of $-1/T$ for different heating rate values, straight lines can be obtained, with their slopes related to the values of the activation energy (see Eq. (11)).

$$\ln(\beta)=\ln\left(\frac{AE_\mathrm{a}}{Rg_{(\alpha)}}\right)-5.331-1.052\frac{E_\mathrm{a}}{RT} \tag{11}$$

The pre-exponential factors can also be inferred based on Eq. (12) (where b is the intercept of the linearized curves) once the form of the reaction model $g_{(\alpha)}$ and the activation energies are known [38].

$$A=\frac{R\exp(b+5.331)g_{(\alpha)}}{E_\mathrm{a}} \tag{12}$$

2.3.2.2. KAS isoconversional model. When only considering the first term of the series depicted in Eq. (7), one can express Eq. (5) in the form:

$$g_{(\alpha)}=\frac{AE_\mathrm{a}}{\beta R}p(u)=\frac{AE_\mathrm{a}}{\beta R}\frac{\exp(-\frac{E_\mathrm{a}}{RT})}{(\frac{E_\mathrm{a}}{RT})^2}=\frac{ART^2}{\beta E_\mathrm{a}}\exp(-\frac{E_\mathrm{a}}{RT}) \tag{13}$$

The expression of the linear integral isoconversional model developed by Kissinger-Akahira-Sunose for a given conversion degree α and a heating rate β then follows a relation of the type:

$$\ln\left(\frac{\beta}{T^2}\right)=\ln\left(\frac{AR}{E_\mathrm{a}g(\alpha)}\right)-\frac{E_\mathrm{a}}{RT} \tag{14}$$

By plotting $\ln\left(\beta/T^2\right)$ as a function of $-1/T$ for different heating rates, straights are obtained, with their slopes allowing to infer the activation energy values for each given conversion degree α. As far as the pre-exponential factors are concerned, they can be estimated, as in the case of the OFW model, based on the intercept of the straight lines once the form of the reaction model $g(\alpha)$ and the activation energies are known (see Eq. (15)).

$$A=\frac{E_\mathrm{a}\exp(b)g(\alpha)}{R} \tag{15}$$

2.3.3. Master plot

In an attempt to select the most suitable reaction model, Sánchez-Jiménez *et al.* [60] proposed a calculation procedure con-

sisting in transforming measured data into an experimental master plot independent of the experimental conditions. This master plot is then compared with theoretical master plots drawn by assuming certain reaction models (see Table 2) so as to determine, by means of a simple graphical procedure, the most adapted kinetic model. To this end, one must first introduce a so-called generalized time, θ, written as:

$$\theta = \int_0^t \exp\left(-\frac{E_a}{RT}\right)\mathrm{d}t \tag{16}$$

whose derivative over t leads to:

$$\frac{\mathrm{d}\theta}{\mathrm{d}t} = \exp\left(-\frac{E_a}{RT}\right) \tag{17}$$

By combining $\mathrm{d}\alpha/\mathrm{d}t$ from Eq. (2) and $\mathrm{d}\theta/\mathrm{d}t$ from Eq. (17), $\mathrm{d}\alpha/\mathrm{d}\theta$ can be reformulated as follows:

$$\frac{\mathrm{d}\alpha}{\mathrm{d}\theta} = \frac{A\exp\left(-E_a/RT\right)f_{(\alpha)}}{\exp\left(-E_a/RT\right)} = Af(\alpha) \tag{18}$$

For a single-step process, the expression of the reaction model is invariable. Using a reference point at α = 50%, one obtains:

$$\frac{\left(\frac{\mathrm{d}\alpha}{\mathrm{d}\theta}\right)_\alpha}{\left(\frac{\mathrm{d}\alpha}{\mathrm{d}\theta}\right)_{50\%\,\mathrm{theo}}} = \frac{f(\alpha)}{f(50\%)} \tag{19}$$

Expressing the generalized reaction rate as:

$$\frac{\mathrm{d}\alpha}{\mathrm{d}\theta} = \frac{\mathrm{d}\alpha}{\mathrm{d}t}\exp\left(\frac{E_a}{RT}\right) \tag{20}$$

the relationship between the generalized reaction rate and the experimental data is defined as follows:

$$\frac{\left(\frac{\mathrm{d}\alpha}{\mathrm{d}\theta}\right)_\alpha}{\left(\frac{\mathrm{d}\alpha}{\mathrm{d}\theta}\right)_{50\%\,\mathrm{exp}}} = \frac{\left(\frac{\mathrm{d}\alpha}{\mathrm{d}t}\right)_\alpha}{\left(\frac{\mathrm{d}\alpha}{\mathrm{d}t}\right)_{50\%}}\frac{\exp\left(\frac{E_a}{RT}\right)}{\exp\left(\frac{E_a}{RT_{50\%}}\right)} \tag{21}$$

By comparing the theoretical curves with experimental ones whose plotting requires an estimation of E_a through model-free methods under non-isothermal conditions, the most suited reaction model (*i.e.*, the one allowing to obtain the best match) can be identified.

3. Results and Discussion

3.1. Experimental characterization of the pyrolysis of coal, wood and their blends

Data issued from the thermogravimetric analyses of coal, wood and their blends for heating rates comprised between 5 °C·min^{-1} and 30 °C·min^{-1} are reported in Fig. 1. As can be seen by looking at the mass loss (TG) and mass loss rate (dTG) curves, results obtained for a given feedstock (*i.e.*, coal, wood or their blends) at different heating rates are relatively similar, while they significantly differ from one fuel to another. To better figure out this aspect, the characteristic pyrolysis temperatures which have been measured are reported in Table 3, noting that the initial and final temperatures (noted $T_{i,10\%}$ and $T_{f,90\%}$ therein) have been estimated based on conversion degrees of 10% and 90%, respectively.

The decomposition of poplar wood typically takes place at lower temperatures and within a narrower range. Indeed, the initial and final pyrolysis temperatures are respectively comprised between 252–291 °C and 391–416 °C, depending on the heating rate, thus corresponding to a temperature range of around 130 °C. In comparison, the decomposition of the coal-containing samples occurs within a larger temperature domain (around 300 °C). The initial decomposition temperature of coal is around 47 °C higher than that of wood, while the final one is at least 209 °C higher. The above observations corroborate the results reported in different studies pertaining to the comparison of the decomposition temperatures of a large variety of coal and biomass types [2,10,13,15,18,19,63]. Such different pyrolysis behaviors may be related to the distinct chemical features of coal and wood. The strong single or double bonds between highly cross-linked aromatic clusters of coal are indeed more difficult to break as their bond energies can reach up to 1000 kJ·mol^{-1}. Consequently, higher temperatures (*i.e.*, more energy) are usually required to decompose coal [10,15,18,64].

On the other hand, biomass consists of a mixture of three biopolymers, namely, cellulose, hemicellulose and lignin. Although these different components are characterized by distinct decomposition temperature ranges, their macromolecular structure is mainly linked by weak ether bonds whose energies are typically comprised between 380 and 420 kJ·mol^{-1} [15]. Lower temperatures (mostly below 400 °C) are thus required to decompose the main components of woody biomass. This has been particularly illustrated by Kastanaki *et al.*, who fitted dTG curves obtained with different biomass materials using a kinetic model involving three independent parallel reactions. By doing so, they estimated that the temperature range of the three biopolymers should be comprised between 230 and 350 °C for hemicellulose, 280 and 400 °C for cellulose, against 200 and 550 °C for lignin [65].

The graphs in Fig. 1 also illustrate that the greater the mass fraction of wood in blended samples, the less the remaining solid residue, regardless of the heating rate considered. This may be related to the inherent properties of wood, which presents a much higher volatile content (see Table 1). Regarding the temperature characterizing the maximal mass loss rates, distinct behaviors are observed depending on the considered fuel. For instance, coal and wood dTG curves exhibit only one peak, against two for the coal/wood mixtures. Furthermore, the greater the heating rate, the higher the mass loss rate, as exemplified in the case of coal, whose maximal decomposition rate is 5 times higher (*i.e.*, from − 0.62%·min^{-1} to − 3.14%·min^{-1}) when increasing the heating rate from 5 to 30 °C·min^{-1} (see Table 3). In comparison, the decomposition of wood is shown to occur more rapidly, with dTG values of − 3.85%·min^{-1} and −21.64 %·min^{-1} for heating rates of 5 and 30 °C·min^{-1}, respectively (see Table 3). This observation is actually consistent with the higher volatile content of the investigated biomass (see Table 1), as well as with the above-mentioned narrower decomposition temperature range.

Based on the pyrolysis behavior of the pure feedstocks, adding wood to coal quite logically induces a reduction of the initial and final pyrolysis temperatures. This is particularly notable in the case of the blend containing 20% of biomass, whose $T_{i,10\%}$ values become closer to those of wood (see Table 3). As mentioned above, blended samples show two dTG peaks, which is commonly observed in TGA experiments conducted with coal/wood mixtures [2,10,13,66]. This may be related to the fact that the whole mass loss curve can be considered as a combination of the TGA curves representing the decomposition of both the individual feedstocks. This is confirmed in the present work by the fact that the two peaks evidenced on the graphs of Fig. 1 are well correlated with the maximal mass loss rates observed in the case of raw wood and coal samples. It is moreover noteworthy that the temperatures (T_p) for which these dTG peaks are recorded are close to those for which the maximal mass loss rates are measured in the case of wood and coal (see Table 3). It can also be noted that increasing the blending ratio of wood leads to an enhancement of the height of the dTG peak corresponding to the decomposition of wood while consequently

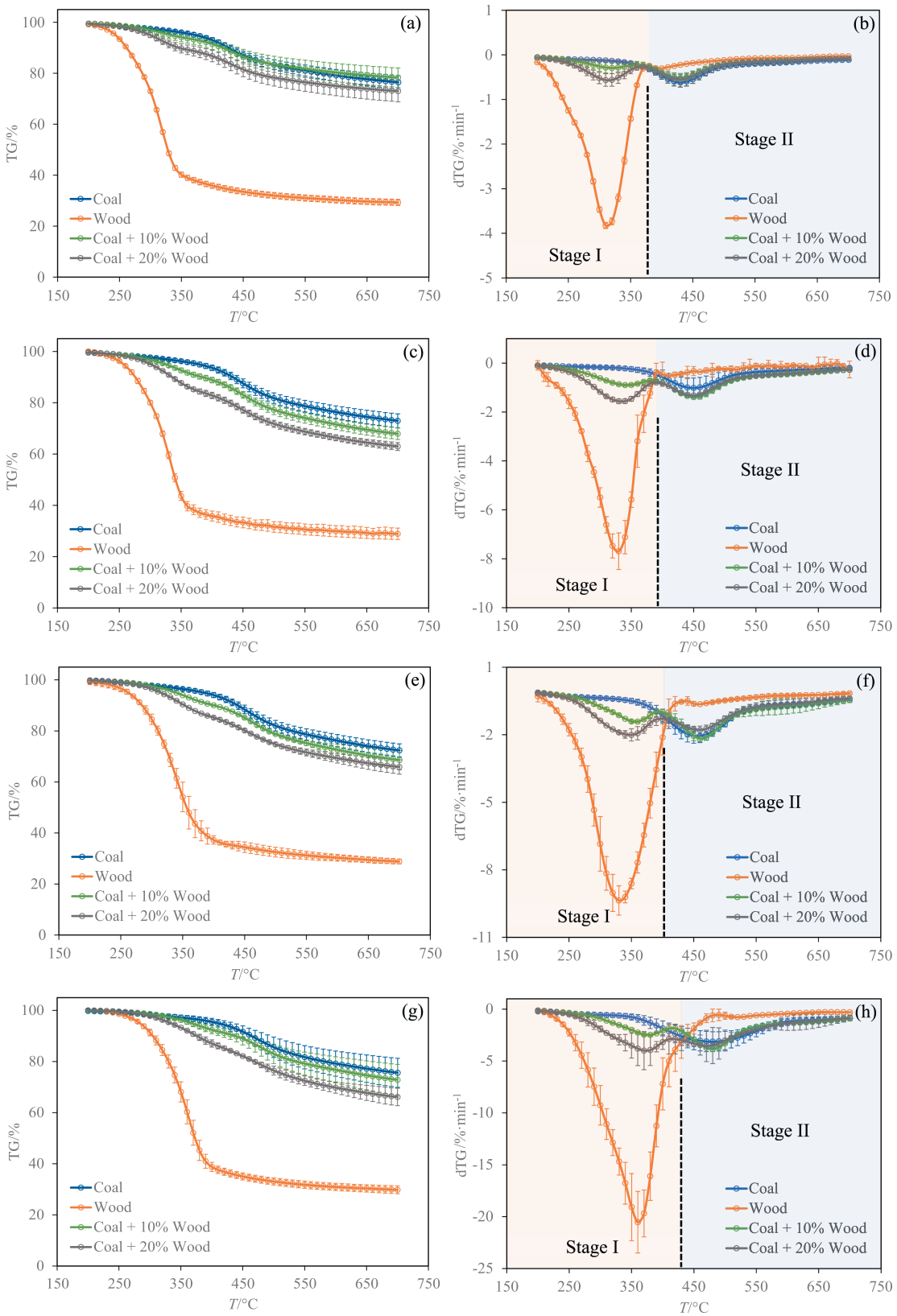

Fig. 1. Evolutions of mass loss (TG) and derivate mass loss rate (dTG) as a function of the temperature for heating rates of 5 °C·min^{-1} (a and b), 10 °C·min^{-1} (c and d), 15 °C·min^{-1} (e and f) and 30 °C·min^{-1} (g and h).

reducing the residual mass. Basically, the mechanism and kinetics underlying the co-pyrolysis process can be divided into two main stages corresponding to the biomass and coal decomposition, respectively. A temperature limit can then be defined to separate the reaction stage for which the biomass decomposition prevails (referred to as stage I) from the one for which the decomposition of coal controls the main process (noted stage II). Based on the data obtained herein, this speculative limit, which roughly corresponds

Table 3
Characteristic decomposition temperatures, maximal mass loss rate and residual mass at 700 °C for coal, biomass and their blends at each studied heating rate

	5 °C·min^{-1}					10 °C·min^{-1}				
	$T_{i,10\%}$ /°C	$T_{f,90\%}$ /°C	T_p/°C	dTG_{max}/ %·min^{-1}	$TG_{700°C}$/% (mass)	$T_{i,10\%}$ /°C	$T_{f,90\%}$ /°C	T_p/°C	dTG_{max}/ %·min^{-1}	$TG_{700°C}$/% (mass)
Coal	294.1 (±2.1)	610.2 (±1.1)	430 (±1)	−0.62 (±0.10)	76.5 (±2.6)	315.1 (±7.9)	617.3 (±3.2)	452 (±7)	−1.03 (±0.41)	73.0 (±2.7)
Wood	252.4 (±0.3)	391.1 (±0.4)	315 (±2)	−3.85 (±0.08)	29.3 (±1.2)	266.6 (±2.9)	394.5 (±15.0)	329 (±10)	−7.80 (±0.75)	28.9 (±2.2)
Coal + 10% Wood	282.2 (±5.8)	594.3 (±2.4)	321 (±2), 431 (±1)	−0.29 (±0.13), −0.52 (±0.10)	78.3 (±4.2)	299.4 (±11.1)	608.9 (±12.6)	347 (±4), 452 (±10)	−0.91 (±0.07), −1.40 (±0.08)	67.9 (±2.3)
Coal + 20% Wood	271.3 (±0.1)	576.8 (±0.1)	315 (±1), 430 (±1)	−0.57 (±0.14), −0.55 (±0.10)	73.0 (±3.8)	288.0 (±4.5)	591.1 (±18.0)	336 (±8), 452 (±5)	−1.59 (±0.10), −1.33 (±0.02)	63.0 (±1.5)
	15 °C·min^{-1}					30 °C·min^{-1}				
	$T_{i,10\%}$ /°C	$T_{f,90\%}$ /°C	T_p/°C	dTG_{max}/ %·min^{-1}	$TG_{700°C}$/% (mass)	$T_{i,10\%}$ /°C	$T_{f,90\%}$ /°C	T_p/°C	dTG_{max}/ %·min^{-1}	$TG_{700°C}$/% (mass)
Coal	322.4 (±8.9)	623.3 (±7.7)	458 (±6)	−2.07 (±0.30)	72.4 (±2.5)	339.3 (±10.7)	628.2 (±3.8)	481 (±6)	−3.14 (±0.96)	75.6 (±5.7)
Wood	273.1 (±0.3)	414.2 (±2.1)	332 (±12)	−9.42 (±0.65)	28.9 (±1.0)	291.4 (±0.3)	415.9 (±12.3)	357 (±13)	−21.64 (±3.10)	29.8 (±1.6)
Coal + 10% Wood	313.0 (±4.0)	617.3 (±9.3)	357 (±3), 463 (±5)	−1.43 (±0.05), −2.19 (±0.14)	68.6 (±3.8)	332.1 (±4.3)	626.9 (±0.1)	378 (±0), 482 (±12)	−2.50 (±0.88), −3.87 (±1.80)	72.9 (±6.0)
Coal + 20% Wood	297.5 (±6.2)	596.4 (±18.2)	344 (±10), 463 (±9)	−2.03 (±0.27), −1.79 (±0.20)	65.9 (±2.8)	316.2 (±10.3)	604.3 (±13.5)	373 (±11), 492 (±14)	−4.00 (±1.85), −3.31 (±1.51)	66.1 (±3.4)

to the temperature for which the dTG curves related to wood and coal intersect, as depicted in Fig. 1(b), 1(d), 1(f) and 1(h), can be estimated to be around 400 °C (with values ranging from 380 to 430 °C for β values comprised between 5 and 30 °C·min^{-1}, respectively). This result is actually well in line with the observations by Masnadi *et al.* [19], in which the co-pyrolysis of coal with switchgrass or pine sawdust was decomposed into two main reaction stages (in addition to drying below 200 °C). These authors particularly linked both reaction stages, which can be distinguished when the absolute slopes of the weight loss profiles start to decrease, to the devolatilization of the main biomass components between ~ 200 and 400 °C, followed by the emission of heavier hydrocarbons issued from the fossil fuel above 475 °C, as observed herein.

3.2. Synergistic effects related to co-pyrolysis

The possible synergies that may occur when different feedstocks are co-pyrolyzed have been subject to ever increasing research during the last few years as such effects are likely to improve the yields of gaseous and volatile species and/or enhance those of target chemicals [14]. These synergistic effects can be observed based on TGA results as they may lead to a higher mass loss measurement when two feedstocks are co-pyrolyzed as compared to the sum of the mass losses assessed when both feedstocks are pyrolyzed separately. Furthermore, a decrease of the activation energies can also be highlighted as a result of these synergies. Based on the TGA results of Fig. 1, one can clearly note that the mass loss curves of blended samples fall between those of coal and wood. This observation, however, does not necessarily point to the presence or absence of synergistic effects. We therefore estimated the deviations (dW) between measured dTG values (noted $dTG_{exp,blend}$) and theoretically calculated ones (based on a simple algebraic sum in which x_{wood} denotes the mass fraction of wood) using Eq. (22) [12,15,20,21]:

$$dW = dTG_{exp,blend} - [x_{wood}dTG_{wood} + (1 - x_{wood})dTG_{coal}] \quad (22)$$

Negative deviations suggest that the blending of wood and coal enhances the decomposition process, thus leading to a quantity of volatile matters emitted exceeding that expected by summing the mass losses related to the individual pyrolysis of both feedstocks.

When looking at the curves depicted in Fig. 2, which represent the evolution of the deviation between measured and calculated dTG values as a function of the temperature for heating rates of 10 and 30 °C·min^{-1}, as examples, one can see that negative dW can be observed during the tests performed with the blends containing 10% and 20% of wood with a heating rate of 10 °C·min^{-1} (see Fig. 2(a), for temperatures comprised between 350 and 700 °C), as well as with the blend containing 20% of biomass for a heating rate of 30 °C·min^{-1} (see discrete points in Fig. 2(b) for temperatures comprised between 400 and 700 °C). Following [12] or [20], these negative deviations thus suggest the possible existence of synergistic effects between coal and poplar wood. Based on the obtained results, it is, however, difficult to draw any clear-cut conclusion in that regard. Indeed, the estimation of negative dW values is not evident for all samples and thermal conditions, especially when considering the uncertainties related to dTG values measured herein (see the error bars plotted in Fig. 1), which thus propagate when estimating the uncertainties encompassing dW (see the error bars depicted in Fig. 2). This therefore makes the identification of synergistic effects based on Eq. (22) somewhat difficult. This may especially explain why diverging trends have sometimes been reported in the literature. Indeed, while some studies have concluded that no mass loss enhancement could be observed during the co-pyrolysis of coal/biomass blends [2,18,19,20], other works have alternatively demonstrated the contrary [15]. Most of these studies are based solely on one test per sample, however, which is likely to lead to relatively significant uncertainties in the obtained results. This thus justifies the need for investigations, including accurate and/or averaged measured data collected under varied thermal conditions (*i.e.*, different heating rates) as performed herein. With a view to more clearly identifying the existence of synergistic effects, Section 3.3 will be devoted to kinetic analyses aimed at better apprehending the mechanisms involved in the co-pyrolysis of coal and biomass.

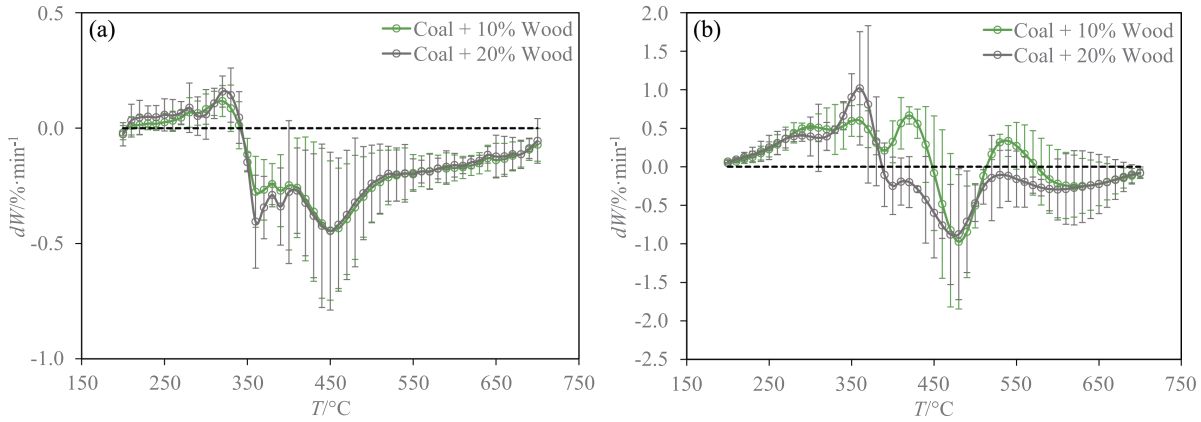

Fig. 2. Deviations (dW) between measured and calculated dTG values for heating rates of: (a) 10 °C·min^{-1} and (b) 30 °C·min^{-1}.

3.3. Kinetic analysis

3.3.1. Modeling of TGA results through isoconversional methods

The kinetic modeling of experimentally assessed results has been achieved using the OFW and KAS isoconversional approaches. To do so, the methodology described in Section 2.3.2 has been applied. As mentioned in Section 2.2, results from 3 tests were averaged to obtain the plots reported in Figs. 3 and 4. Doing so allowed to mitigate the slight deviations observed from test to test due to measurement noise. This therefore enabled obtaining good linear correlations (as exemplified in Figs. 3 and 4), which is very important for assessing accurate kinetic parameters.

As can be seen by looking at the results summarized in Tables 4 and 5, both models lead to very similar E_a values with very high determination coefficients (R^2). As far as the pyrolysis of wood is concerned, inferred activation energies are found to vary within a relatively narrow range. E_a is indeed quite constant for 10%≤ α≤80% ((121.2 ± 4.4) kJ·mol^{-1} and (117.6 ± 4.3) kJ·mol^{-1} considering 95% confidence intervals for the OFW and KAS models, respectively) before rising up to 188.4 kJ·mol^{-1} (OFW) and 186.9 kJ·mol^{-1} (KAS) for α = 90 %.

The overall one-step pyrolysis process observed for conversion degrees comprised between 10% and 80% is actually in line with the relative simplicity of the reactions involved in the decomposi-

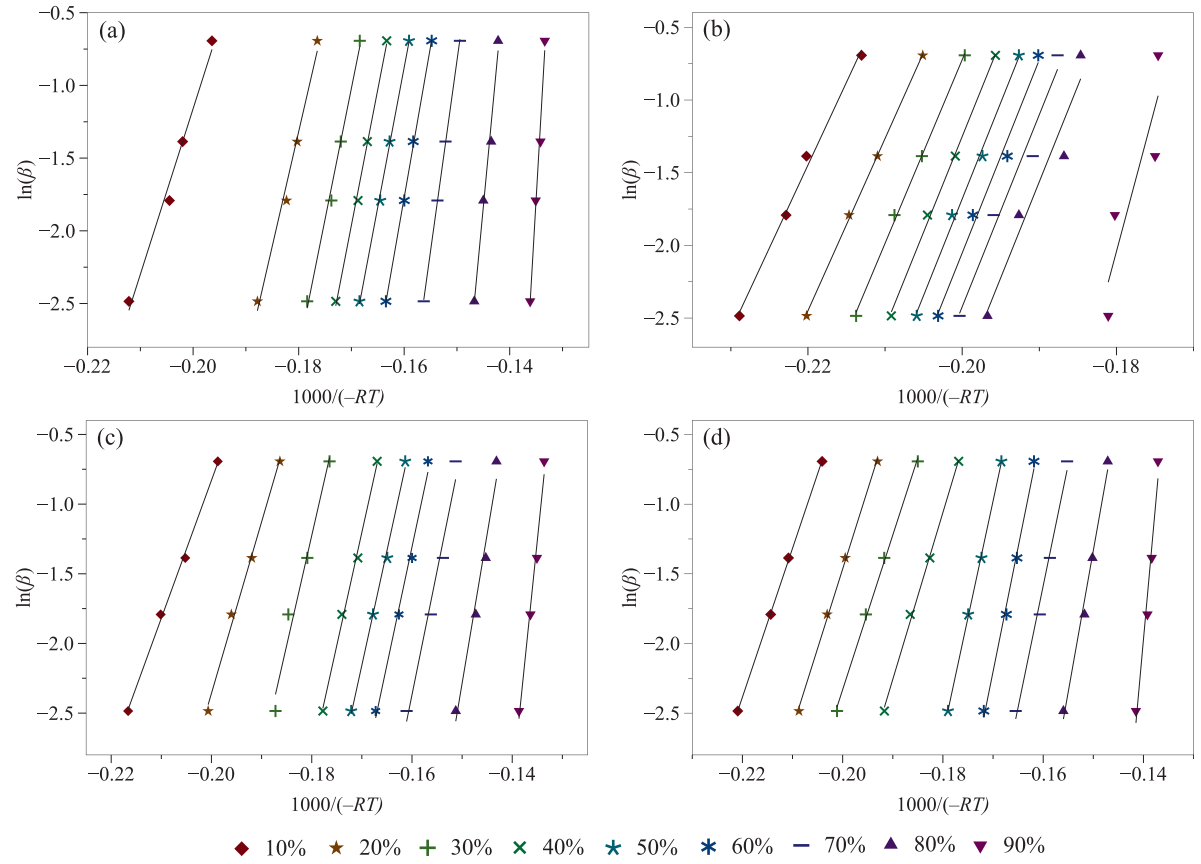

Fig. 3. Modeling results issued from the use of the OFW model for: (a) coal, (b) wood, (c) coal + 10 % wood and (d) coal + 20 % wood.

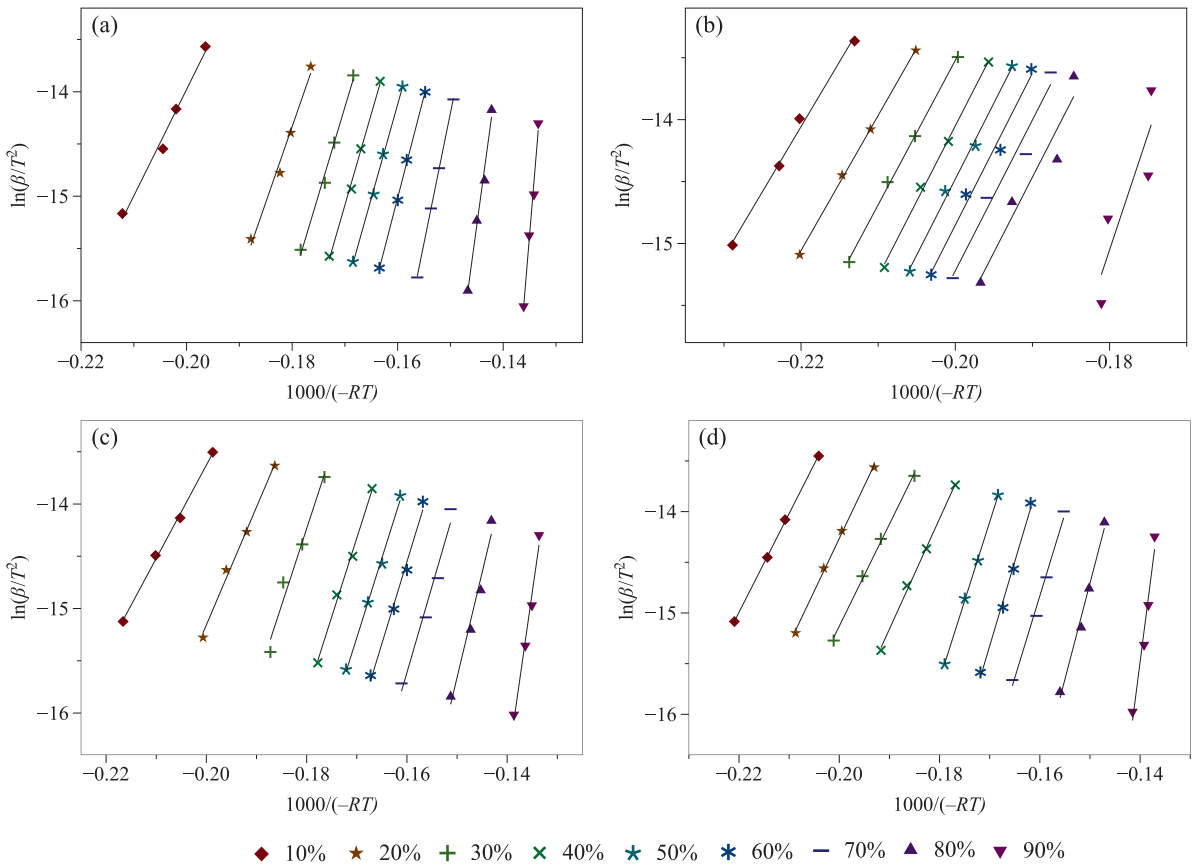

Fig. 4. Modeling results issued from the use of the KAS model for: (a) coal, (b) wood, (c) coal + 10 % wood and (d) coal + 20 % wood.

Table 4
Activation energies assessed using the OFW model

α	Coal		Wood		Coal + 10% Wood		Coal + 20% Wood	
	E_a/kJ·mol^{-1}	R^2	E_a/kJ·mol^{-1}	R^2	E_a/kJ·mol^{-1}	R^2	E_a/kJ·mol^{-1}	R^2
10%	108.3	0.9869	108.4	0.9945	94.1	0.9979	101.6	0.9998
20%	149.8	0.9891	112.6	0.9994	116.9	0.9948	108.4	0.9987
30%	171.4	0.9934	120.0	0.9986	149.8	0.9739	105.6	0.9983
40%	177.7	0.9967	124.8	0.9978	154.3	0.9959	113.9	0.9981
50%	182.7	0.9983	126.1	0.9955	156.3	0.9963	159.1	0.9995
60%	197.7	0.9991	126.3	0.9876	160.8	0.9900	169.7	0.9940
70%	248.5	0.9997	125.6	0.9718	168.8	0.9742	165.8	0.9906
80%	364.6	0.9879	125.5	0.9394	203.9	0.9756	192.5	0.9900
90%	595.8	0.9882	188.4	0.8050	331.8	0.9859	379.4	0.9727

Table 5
Activation energies assessed using the KAS model

α	Coal		Wood		Coal + 10% Wood		Coal + 20% Wood	
	E_a/kJ·mol^{-1}	R^2	E_a/kJ·mol^{-1}	R^2	E_a/kJ·mol^{-1}	R^2	E_a/kJ·mol^{-1}	R^2
10%	104.2	0.9848	104.9	0.9933	89.4	0.9975	97.4	0.9997
20%	146.6	0.9946	109.0	0.9993	112.7	0.9937	104.1	0.9984
30%	168.8	0.9959	116.6	0.9983	146.7	0.9698	100.7	0.9979
40%	175.0	0.9972	121.5	0.9974	150.7	0.9953	108.9	0.9976
50%	179.9	0.9981	122.6	0.9947	152.4	0.9958	155.8	0.9995
60%	195.4	0.9991	122.7	0.9855	156.8	0.9885	166.5	0.9931
70%	248.3	0.9999	121.8	0.9670	164.8	0.9703	161.9	0.9892
80%	369.7	0.9877	121.5	0.9292	201.0	0.9723	189.3	0.9886
90%	611.9	0.9880	186.9	0.7862	334.4	0.9847	384.7	0.9707

tion of the main wood materials (cellulose and hemicellulose). On the other hand, the higher E_a values estimated for $\alpha > 80\%$ may be related to the decomposition of lignin, which contains more rigid carbon–carbon linkages whose breakage requires more energy, and thus, higher temperatures [4].

As compared to wood, the activation energies determined for coal-containing samples vary to a much greater extent. E_a indeed rises from 108.3 to 595.8 kJ·mol^{-1} based on the OFW model, against 104.2 to 611.9 kJ·mol^{-1} with the KAS one for pure coal. Here again, this trend is coherent with respect to the complexity of the coal chemical structure as well as with the complexity of related reaction mechanisms which comprise dehydration and degassing stage for temperatures below ~ 240 °C, initial pyrolysis between ~ 240 and ~ 350 °C, main pyrolysis which extends from ~ 350 to ~ 700 °C and secondary degassing with polycondensation above ~ 700 °C [2,10,14,46,67,68]. It is further of interest to mention that the order of magnitudes of the E_a values estimated herein are in good agreement with those reported in the literature (*i.e.*, between 100 and 300 kJ·mol^{-1} for biomass [4] and from 100 to 600 kJ·mol^{-1} for coal [9]). One can still note that higher activation energies have sometimes been reported in the literature with respect to poplar wood (233 kJ·mol^{-1} on average for $5\% \leq \alpha \leq 80\%$ using the Friedman method in [69] against mean values of 197.73 and 198.00 kJ·mol^{-1} in [70] when implementing the OFW and KAS modeling approaches). In an attempt to interpret these discrepancies, different options have been considered. Firstly, the possible effect of the sample mass on the TG results has been examined. Indeed, the sample mass times the heating rate ($m\beta$) set herein exceeds the initial guess of 100 mg·°C·min^{-1} recommended in [71], especially for measurements conducted with a β value of 30 °C·min^{-1}. This could therefore induce heat and mass transfer limitations during thermal degradation tests, which are prone to influence the so-obtained results. Nevertheless, the data from [69] and [70] are issued from experiments conducted using quite similar operating conditions (*i.e.*, 10 mg of sample with maximum heating rates of 25 °C·min^{-1} [69] and 30° C·min^{-1} [70]). This therefore tends to discard any heat transfer issue likely to account for the differences observed between the tests carried out herein and those performed in [69,70]. This conclusion is, moreover, corroborated by the fact that excluding the results obtained with a heating rate of 30 °C·min^{-1} from the kinetic analysis conducted in this work would lead to mean E_a values of (123.3 ± 11.4) kJ·mol^{-1} and (119.7 ± 11.8) kJ·mol^{-1} for $10\% \leq \alpha \leq 90\%$ with the OFW and KAS models, respectively. As can be seen, these values are quite similar to the mean activation energies of (128.6 ± 13.6) kJ·mol^{-1} and (125.3 ± 14.0) kJ·mol^{-1} estimated when taking the highest β value into account. Actually, the mean relative deviations between E_a inferred whether considering the heating rate of 30 °C·min^{-1} or not is less than 4.6% for all investigated samples. As a consequence, passing from a maximum $m\beta$ of 300 to 150 mg·°C·min^{-1} clearly has no significant impact on the inferred kinetic parameters, hence discarding any heat and mass transfer limitations. It is of interest to note that this observation is also supported by the results of [53], who analyzed the pyrolysis kinetics of poplar biomass. [53] indeed found no significant differences between the thermograms obtained when using sample masses below 10 mg and between 30 and 70 mg, for heating rates up to 50 °C·min^{-1}. To conclude, it is noteworthy that different studies which are based on isoconversional methods have alternatively reported mean activation energies below 150 kJ·mol^{-1} [37] and even below 100 kJ·mol^{-1} [72] for lignocellulosic biomass. In the case of poplar wood, [73] especially found activation energies going from 107.9 to 209.5 kJ·mol^{-1} for $5\% \leq \alpha \leq 70\%$ when using the OFW model against values comprised between 105.0 and 209.9 for the KAS method, which is relatively close to the order of magnitudes estimated herein (the relative deviations between the mean E_a values from [73] and those inferred in the present work being indeed of the order of ~ 20%). Finally, [53] has reported that the activation energies related to the pyrolysis of poplar wood significantly depend on the feedstock genotype, thus leading to values that can possibly range from 108 to 320 kJ·mol^{-1}. All these observations therefore tend to corroborate the consistency of the kinetic analysis conducted herein as well as the relevance of the so-derived kinetic parameters.

Regarding blended samples, the activation energy decreases when wood is added to coal (see Tables 4 and 5 as well as Fig. 5), which is particularly notable with the blend containing 20% of biomass for $10\% < \alpha < 40\%$. The fact that the curves depicting the evolution of E_a as a function of α for blended samples are significantly below the curve obtained for pure coal despite the relatively low blending ratios (*i.e.*, 10% and 20%) suggests the possible presence of synergistic effects whose mechanisms will be discussed in greater detail in Section 3.3.4. This conclusion is especially corroborated by the fact that the E_a values for the blend containing 20% of biomass are even lower than those inferred in the case of pure wood for conversion degrees comprised between 20% and 40% (see Tables 4 and 5 and Fig. 5). This observation thus tends to corroborate the presence of synergies which expand the degradation rate of the blended sample especially for low conversion degrees (*i.e.*, for temperatures below 450 °C). While being consistent with the fact that synergistic effects are known to decrease the activation energy of the pyrolysis reactions, so-enhancing the yields of volatile species, the apparently stronger impact of such a phenomenon in the low temperature regime also falls in line with trends previously reported in the literature [3,9].

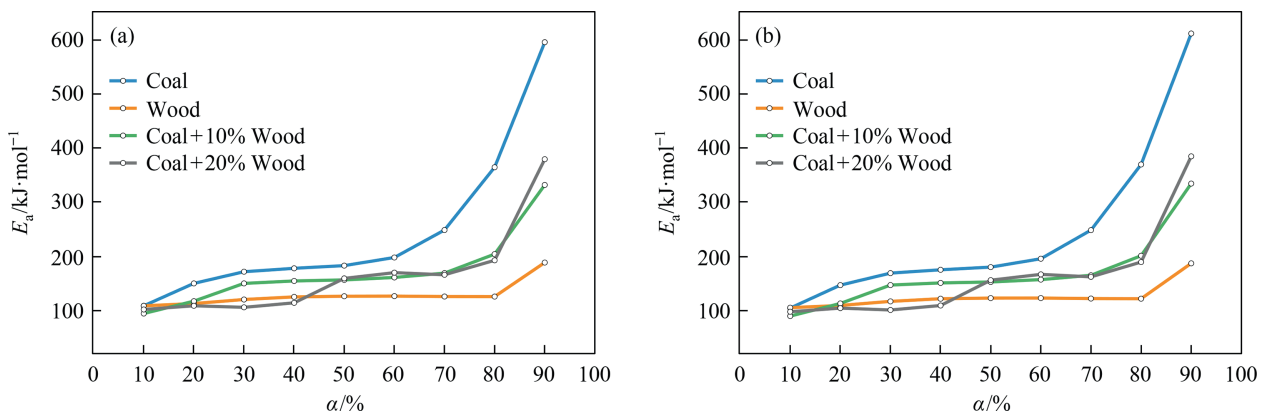

Fig. 5. Evolutions of the activation energy (E_a) as a function of the conversion degree (α) for: (a) the OFW and (b) the KAS models.

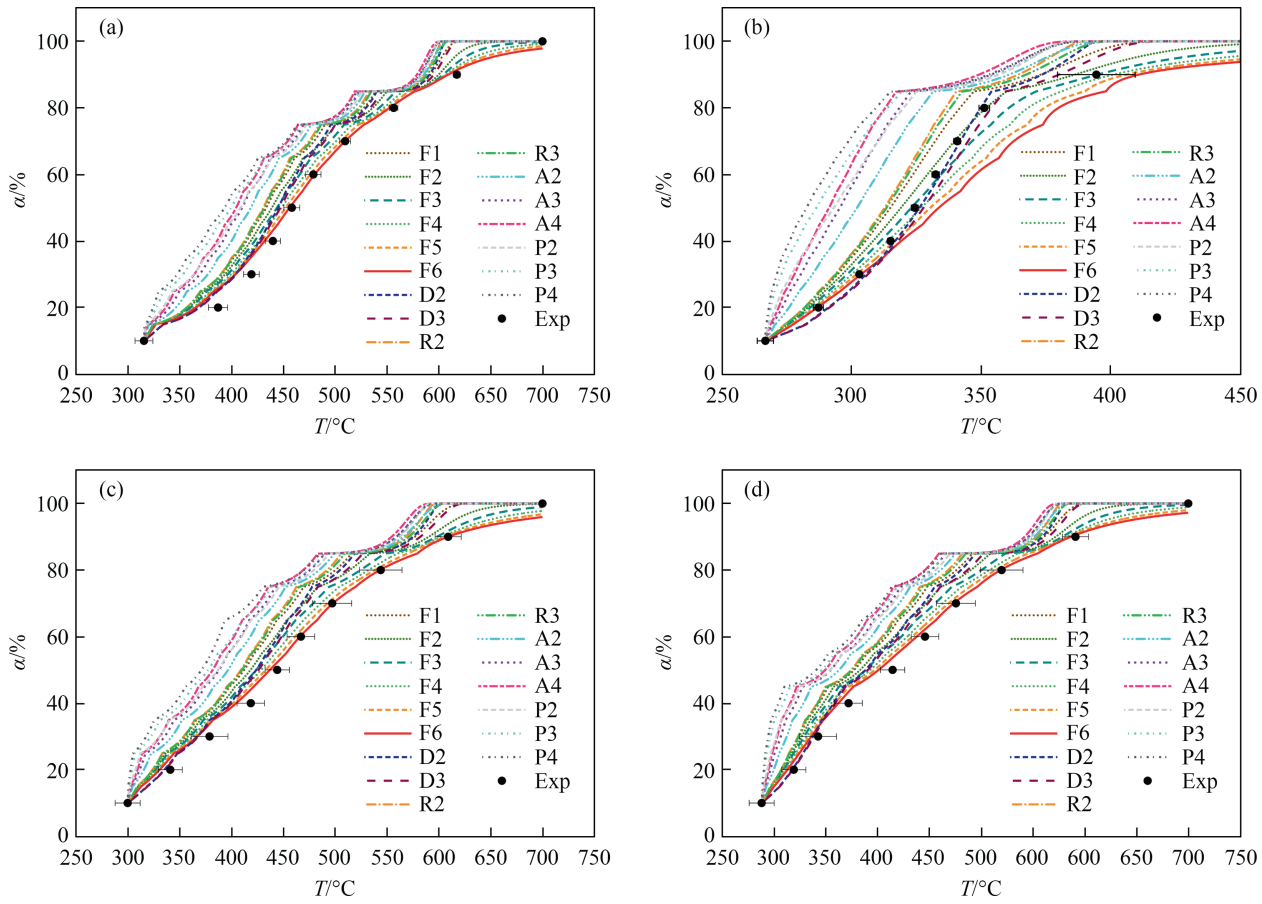

Fig. 6. Evolutions of the conversion degree as a function of the temperature for a heating rate of 10 °C·min^{-1} in the case of: (a) coal, (b) wood, (c) coal + 10% wood and (d) coal + 20% wood. Comparison of experimental data (noted 'Exp') with predicted ones issued from the use of the OFW model.

To conclude, it is of interest to note that the activation energies rise monotonously with increasing conversion degrees as depicted in Fig. 5 (except for the wood sample whose pyrolysis mainly follows a one-step process characterized by a quite constant E_a value for $10\% \leq \alpha \leq 80\%$). Such a trend is actually consistent with what would be anticipated, as well as with the observations made in [74] as an example. It is indeed generally admitted that low E_a values relate to reactions occurring at low temperatures, and vice versa. The variations of E_a assessed in the literature when using model-free methods, however, do not always follow this general trend, thus making the interpretation of obtained kinetic results sometimes quite difficult. These unexpected results can often be traced to uncertainties and fluctuations encompassing recorded data, thus explaining why results from three TGA tests have been averaged in the present work to tackle this issue. Consequently, and even though determination coefficients above 0.9 are generally considered as satisfactory, some researchers still consider that model-free methods are only applicable on a narrow range of conversion degrees (up to 60%–70%) [75–78]. Finally, many studies focusing on model-free methods only lead to the estimation of E_a values whose meaning and validity are not always verified. In fact, inferring solely activation energies is insufficient to reproduce kinetic data, which thus explains why comparisons between measured data and predicted ones issued from isoconversional kinetic analyses are somewhat scarce. Consequently, a procedure aimed at ruling on the predictive character of the kinetic parameters estimated throughout the present work has been implemented, as detailed in Section 3.3.2.

3.3.2. Prediction of pyrolysis kinetics and validation of assessed kinetic parameters

In addition to the activation energies inferred in Section 3.3.1 (see Tables 4 and 5), the values of the pre-exponential factor (A) integrated within the expression of the rate constant also need to be assessed to simulate experimental results by means of model-free methods. To that end, 16 reaction models including the F1, F2, F3, F4, F5, F6, D2, D3, R2, R3, A2, A3, A4, P2, P3 and P4 ones (see Table 2) were tested with a view to identifying the most suitable $g_{(\alpha)}$ formulation. Using Eqs. (12) and (15) for the OFW and KAS approaches, respectively, a series of pre-exponential factors were derived, as detailed in Tables S1 to S8 provided as Supplementary Material. Integrating the obtained kinetic parameters within Eq. (3) enabled plotting the curves reportd in Figs. 6 and 7 depicting the evolution of the conversion degree as a function of the temperature for a heating rate of 10 °C·min^{-1} as an example. To obtain these graphs, the temperatures reported in Table 3 for a conversion degree of 10% were set as initial reaction temperatures. Calculations were then carried out by applying the kinetic parameters derived for a given α value on a ± 5% conversion degree range (*e.g.*, rate constant parameters estimated for α = 20% were kept constant to perform the calculations for $15\% < \alpha < 25\%$).

The obtained results show that both the OFW and KAS isoconversional models allow correctly simulating the overall evolution of the conversion degree as a function of the temperature, regardless of the sample considered (*i.e.*, coal, wood or their blends). With respect to wood (see Figs. 6(b) and 7(b)), at least two reaction models (*i.e.*, D2 and F2) allow to reproduce satisfactory measured data.

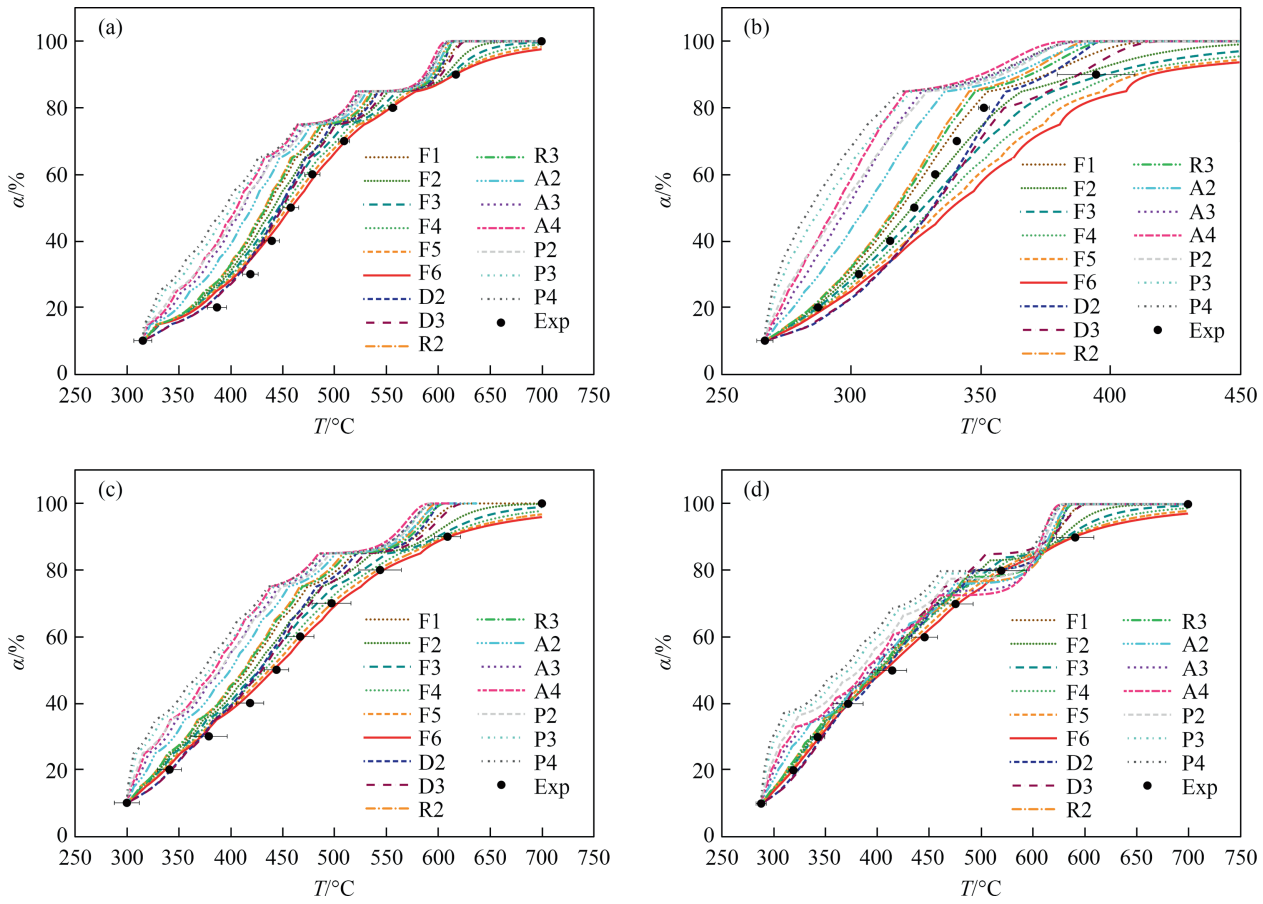

Fig. 7. Evolutions of the conversion degree as a function of the temperature for a heating rate of 10 °C·min^{-1} in the case of: (a) coal, (b) wood, (c) coal + 10% wood and (d) coal + 20% wood. Comparison of experimental data (noted 'Exp') with predicted ones issued from the use of the KAS model.

On the other hand, the F6 model appears to be the most suited for the 3 coal-containing samples.

Based on the kinetic parameters derived from the implementation of the OFW and KAS approaches and on the reaction models identified through Figs. 6 and 7, one can plot the theoretical conversion degree profiles of Fig. 8 which are compared with their experimental counterparts for a heating rate of 10 °C·min^{-1} (profiles corresponding to β values of 5, 15 and 30 °C·min^{-1} being reported, for their part, in Figs. S1 to S3 of the Supplementary Material). Overall, predictions from each model allow obtaining a very good fit with experimental points which thus corroborates the consistency of the modeling procedure implemented herein. The approach selected to identify suitable $g(\alpha)$ formulations has moreover proven to be efficient although another method (the master plot) will still be considered in Section 3.3.3 with the view to confirm obtained results.

3.3.3. Master plot

In this section, the generalized master plot method proposed by Sánchez-Jiménez *et al.* [60] is implemented to the data collected with the wood sample. Indeed, and as noted in Section 2.3.3, this method is only applicable to single-step processes for which the activation energy does not vary with the conversion degree. This condition is only fulfilled with the wood sample for which mean E_a values of (121.2 ± 4.4) kJ·mol^{-1} and (117.6 ± 4.3) kJ·mol^{-1} are estimated for $10\% \leq \alpha \leq 80\%$ with the OFW and KAS models, respectively. The master plot approach was therefore applied only to this feedstock. To this end, measured data were transformed into an experimental master plot following the procedure detailed in Section 2.3.3. They were then compared with theoretical master plots derived from the use of the 16 reaction models previously implemented in Section 3.3.2. As illustrated in Fig. 9, which depicts the results obtained for a heating rate of 10 °C·min^{-1} (data related to β values of 5, 15 and 30 °C·min^{-1} being reported in Figs. S4 to S6 of the Supplementary Material), the models identified in Section 3.3.2 in the case of model-free methods (*i.e.*, D2 (OFW) or F2 (KAS)) allow to satisfactorily reproduce experimental data.

In general, order- and diffusion-based models lead to the best agreement with measured data versus other tested reaction models. This observation is consistent with the conclusions drawn above when implementing isoconversional methods. Furthermore, it is also consistent with results issued from previous studies dealing with biomass pyrolysis, in which order- and diffusion-based models were also identified as being the most suited [33,36,37,39,79]. It can thus be concluded that the calculation procedure proposed in Section 3.3.2 is well applicable as it allowed to obtain consistent results, even though it has seldom been used in the literature. Nevertheless, the master plot also represents a very interesting and efficient approach which allows to identify and select the most adapted reaction model within the context of kinetic analyses, as previously noted by Wang *et al.* in a general review focusing on biomass pyrolysis [4]. Its major limitation, however, lies in the fact that it cannot be applied to multi-step kinetic processes with significant E_a variations as a function of α, as is the case for the coal-containing samples studied in the present work. Despite this limitation, some authors still used the master plot approach to identify reaction mechanisms that allow to account for the pyrolysis of coal and/or coal/biomass blends even

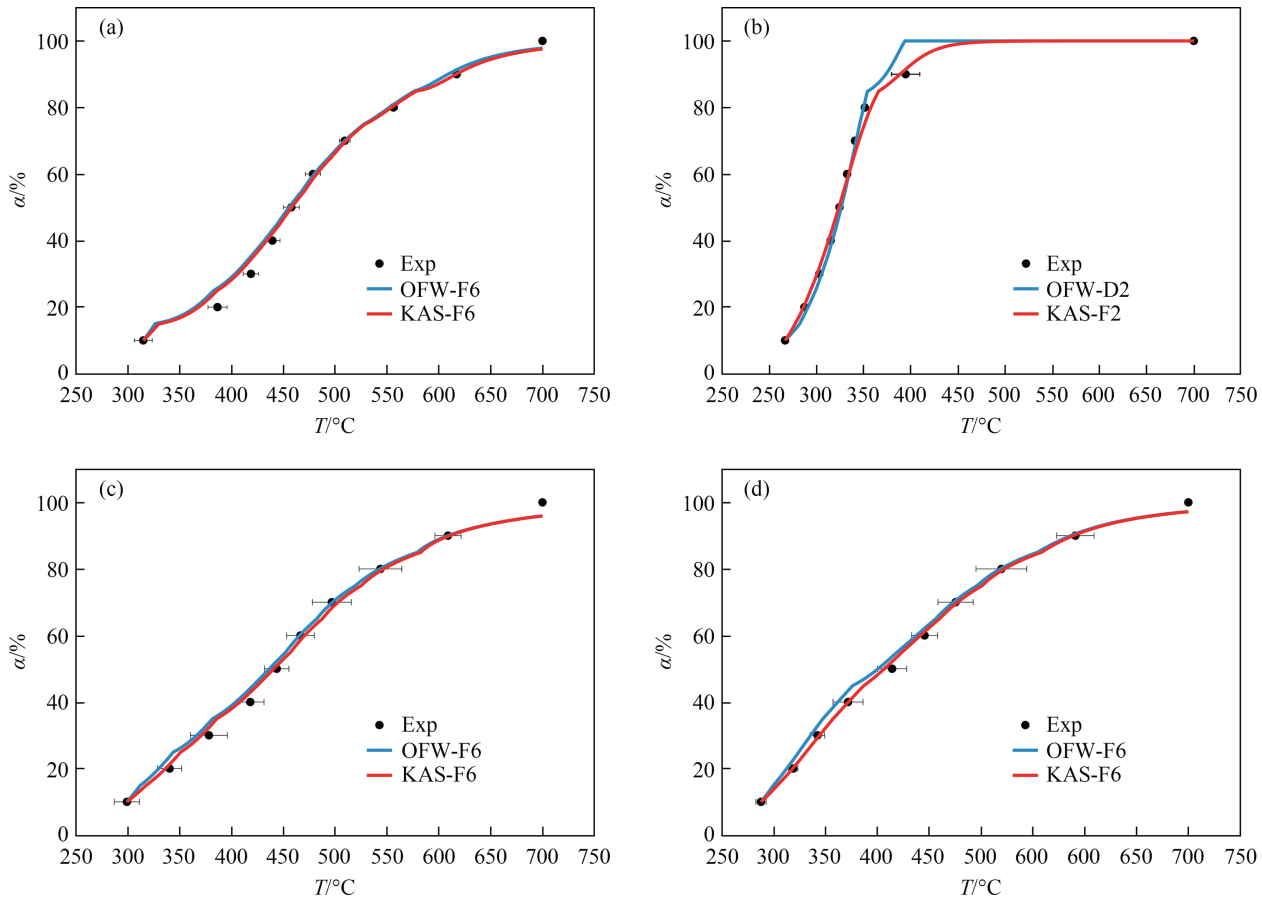

Fig. 8. Evolutions of the conversion degree as a function of the temperature for a heating rate of 10 °C·min^{-1} in the case of: (a) coal, (b) wood, (c) coal + 10% wood and (d) coal + 20% wood. Comparison of experimental data (noted 'Exp') with predicted ones issued from the use of the OFW and KAS models.

with E_a values that vary significantly with α [39,40,80,81]. Doing so for the coal-containing samples while considering α values comprised between 20% and 80% for which the activation energies vary less, the F6 model could be identified as the most suited one. Notwithstanding the agreement with the model identified in Section 3.3.2 as well as with the results from [39,40,80–82] which concluded that nth-order models were the most adapted, it should be recalled that using the master plot method to investigate multi-step reaction mechanisms remains ill adapted. This therefore explains why related results are not reported herein while prompting the need for special caution when analyzing results depicting relatively large variations of the activation energy as a function of the fuel conversion degree.

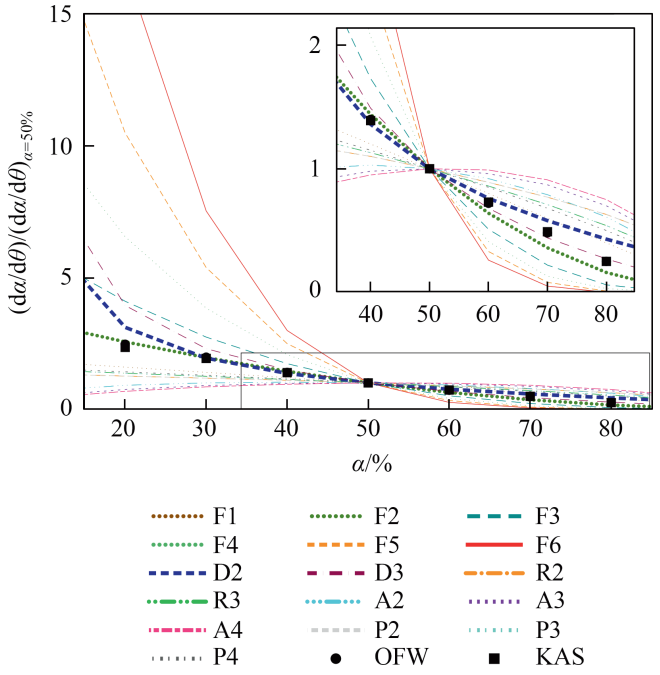

Fig. 9. Comparison of experimental (β = 10 °C·min^{-1}) and theoretical master plots for wood.

3.3.4. Mechanisms underlying synergistic effects

Although the present study contributed to evidencing the probable existence of synergistic effects from a kinetic perspective, analyses aimed at characterizing the composition of devolatilized species are also of major interest to gain fundamental knowledge on the mechanisms at play during the co-pyrolysis of coal and wood. To provide some information in this regard, the present section presents a description of the possible pathways prone to inducing the so-observed synergies. Basically, two main mechanisms represented in Fig. 10 can influence the pyrolysis of blended samples.

First, biomass presents higher H/C and O/C molar ratios than coal (1.41 and 0.65 for the polar wood against 0.77 and 0.11 for the bituminous coal tested herein). As such, biomass is likely to emit more OH and H free radicals prone to inhibiting condensation, recombination and crosslinking reactions [1,9,12–15]. This effect is therefore expected to be mainly active when the blending ratio of wood is sufficiently high. This has been notably demonstrated by Meng *et al.* [1] who studied the co-pyrolysis of platanus wood

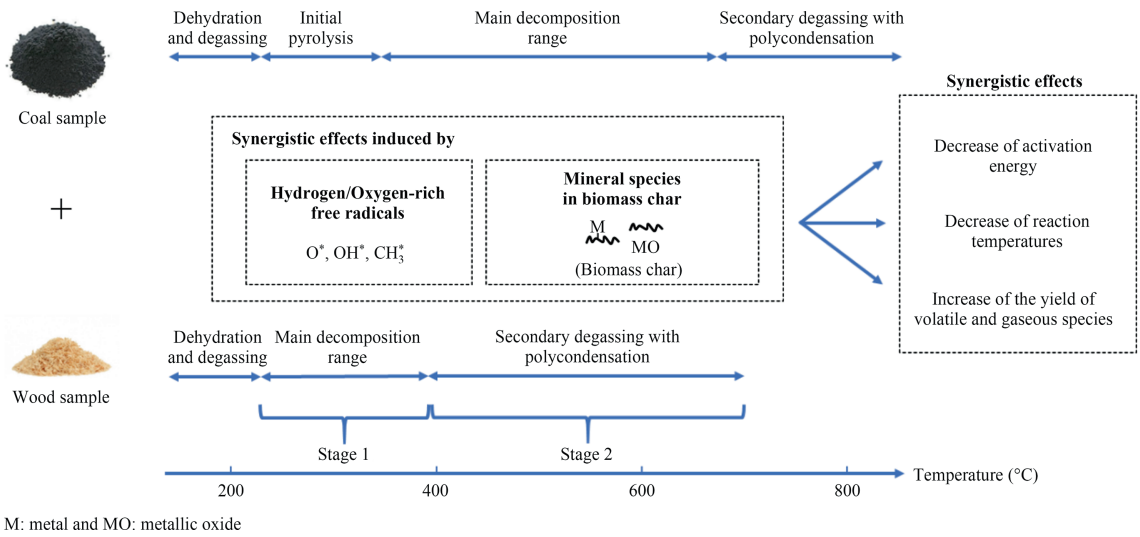

Fig. 10. Possible reaction mechanisms at play during the co-pyrolysis of coal and biomass.

blends with two different rank coals. They indeed observed most obvious synergies during the tests performed using relatively high platanus wood fractions. More recently, Yang *et al.* [14] investigated the co-pyrolysis of walnut shell and coal at five blending mass ratios. They also found that the sample containing the lowest quantity of biomass exhibit the lowest synergies due to low quantities of hydrogen and hydroxyl radicals. Yang *et al.* [14] moreover, showed that the thermal conditions also drastically impact the synergistic effects, which generally occur over a temperature range overlapping the decomposition of both feedstocks. Thus, the reactive free radicals released from the pyrolysis of biomass are expected to react with free radicals issued from the coal pyrolysis, thereby influencing the subsequent pyrolysis reactions. At high temperatures, the synergistic effects are, however, largely reduced since most of the volatiles have been previously released, and the blended solid residues are barely affected [15]. It is thus quite interesting to note that synergies were identified herein during the decomposition of coal (*i.e.*, for α comprised between ~20% and ~40%). The kinetic analysis performed herein (see Section 3.3.1) especially showed that higher decomposition rates and reduced activation energies begin to appear during this specific reaction stage and especially for the 'coal + 20% wood' sample (*i.e.*, for the highest blending ratio which has been tested). E_a values lower than those derived in the case of pure wood were even obtained for α comprised between 20% and 40%. All these observations thus contribute to corroborating the possible existence of synergistic effects during the co-pyrolysis of the La Loma coal with poplar wood.

The second pathway prone to influencing synergies during co-pyrolysis involves mineral species, such as Fe, Ca and K, which are largely present in biomass char. These minerals may in fact act as catalysts during the pyrolysis by enhancing the reactions between volatiles and char to generate lighter molecular compounds [10,12,13,15,66]. Consequently, adding biomass to coal is supposed to enhance the production of tar and gaseous species. This was illustrated by Liu *et al.* [83] who showed that adding CaO, K_2CO_3 and Al_2O_3 to two Chinese coals led to changes in the characteristic decomposition temperatures while decreasing the activation energies of the pyrolysis reactions. They moreover stated that CaO could react with some oxygen functional groups through deoxygenation and deacidification to form CO, while Al_2O_3 could be considered as an active catalyst in de-alkyl and dehydrogenization reactions. Although these different mechanisms cannot be directly shown through kinetic analyses, they may still contribute to the trends seen throughout the present work.

4. Conclusions

The co-pyrolysis of a bituminous coal with poplar wood was experimentally studied by means of thermogravimetric analysis. Obtained *TG* curves illustrated a substantial decrease of the reaction temperatures with the addition of biomass. dTG curves moreover led to the observation of the presence of two peaks that were correlated to the decomposition of both feedstocks (*i.e.*, wood and coal) occurring at relatively low and high temperatures, respectively. The analysis of the dTG curves did not allow to draw clear-cut conclusions regarding the presence of synergistic effects, however. Kinetic analyses were therefore performed using two model-free methods (the OFW and KAS models). A significant decrease of the activation energy was observed when adding wood to coal. Some E_a values inferred for the 'coal + 20% wood' sample were even found to be lower than those estimated for pure wood, thus illustrating probable synergies.

The kinetic analysis that was realized also allowed to assess pre-exponential factors while identifying reaction models suitable for simulating the measured evolution of the conversion degree as a function of the temperature. Results obtained showed that order- and diffusion-based models were the most adapted to satisfactorily reproduce experimental data. More specifically, the F6 model was found to be the most suited to simulate the pyrolysis of coal-containing samples, whereas the D2 and F2 models were found to be well adapted to represent the decomposition of pure wood. As for the master plot, it turned out to be very effective in identifying a proper reaction model similar to those determined when using direct calculation procedures for wood. Finally, the mechanisms underlying the synergistic effects at play during the co-pyrolysis of coal and wood were discussed. Two main reaction pathways involving free radicals and mineral species in wood char were particularly identified in an attempt to explain the experimental observations made throughout the present study.

This work therefore contributes to providing insights regarding the relative impact of adding wood to coal on pyrolysis kinetics. Furthermore, the rate constant parameters derived from the use of the model-free methods should be of help in simulating the co-pyrolysis of poplar wood and bituminous coals under low heating rate conditions. Non-isothermal TGA results have indeed proven to be quite useful for studying and modeling the slow

pyrolysis of solid fuels, as reviewed in [84,85], and illustrated through the different references cited throughout this paper. Besides, different studies have shown that kinetic parameters derived from constant heating rate pyrolysis experiments (as is the case herein, using model-free isoconversional methods) could be used to some extent in order to predict mass losses assessed under other thermal conditions, including other heating rates, as well as isothermal heating conditions [26,86]. Rate constant parameters inferred by TGA analyses can, moreover, be used to properly simulate the slow decomposition of biomass in reactors, as exemplified in [87]. Further works aimed at analyzing the validity of the trends observed herein over an extended range of conditions should, however, be undertaken, especially since industrial fast gasification and combustion reactors typically involve significantly high characteristic temperatures and heating rates [47]. In addition, deriving adapted kinetic triplets to simulate the high heating rate devolatilization process occurring in pulverized fuel boilers for example will require conducting additional studies by coupling TGA and flat-flame reactor measurements, as we recently did in [88], thus paving the way for future work to be undertaken.

Declaration of Competing Interest

The authors declare that they have no known competing financial interests or personal relationships that could have appeared to influence the work reported in this paper.

Acknowledgements

This research has received the support of the French Ministry of Higher Education, Research and Innovation (Ministère de l'Enseignement supérieur, de la Recherche et de l'Innovation).

Supplementary Material

Supplementary data to this article can be found online at https://doi.org/10.1016/j.cjche.2022.10.015.

References

[1] H.Y. Meng, S.Z. Wang, L. Chen, Z.Q. Wu, J. Zhao, Thermal behavior and the evolution of char structure during co-pyrolysis of platanus wood blends with different rank coals from northern China, *Fuel* 158 (2015) 602–611.
[2] K.M. Lu, W.J. Lee, W.H. Chen, T.C. Lin, Thermogravimetric analysis and kinetics of co-pyrolysis of raw/torrefied wood and coal blends, *Appl. Energy* 105 (2013) 57–65.
[3] W. Wang, R. Lemaire, A. Bensakhria, D. Luart, Review on the catalytic effects of alkali and alkaline earth metals (AAEMs) including sodium, potassium, calcium and magnesium on the pyrolysis of lignocellulosic biomass and on the co-pyrolysis of coal with biomass, *J. Anal. Appl. Pyrolysis* 163 (2022) 105479.
[4] S.R. Wang, G.X. Dai, H.P. Yang, Z.Y. Luo, Lignocellulosic biomass pyrolysis mechanism: A state-of-the-art review, *Prog. Energy Combust. Sci.* 62 (2017) 33–86.
[5] Z.G. Huang, J. Zhang, M.M. Pan, Y.H. Hao, R.C. Hu, W.B. Xiao, G. Li, T. Lyu, Valorisation of microalgae residues after lipid extraction: Pyrolysis characteristics for biofuel production, *Biochem. Eng. J.* 179 (2022) 108330.
[6] G. Li, X. Bai, S.H. Huo, Z.G. Huang, Fast pyrolysis of LERDADEs for renewable biofuels, *IET Renew. Power Gener.* 14 (6) (2020) 959–967.
[7] R.P. Anex, A. Aden, F.K. Kazi, J. Fortman, R.M. Swanson, M.M. Wright, J.A. Satrio, R.C. Brown, D.E. Daugaard, A. Platon, G. Kothandaraman, D.D. Hsu, A. Dutta, Techno-economic comparison of biomass-to-transportation fuels *via* pyrolysis, gasification, and biochemical pathways, *Fuel* 89 (2010) S29–S35.
[8] T.R. Brown, R. Thilakaratne, R.C. Brown, G.P. Hu, Techno-economic analysis of biomass to transportation fuels and electricity *via* fast pyrolysis and hydroprocessing, *Fuel* 106 (2013) 463–469.
[9] S.M. Gouws, M. Carrier, J.R. Bunt, H.W.J.P. Neomagus, Co-pyrolysis of coal and raw/torrefied biomass: A review on chemistry, kinetics and implementation, *Renew. Sustain. Energy Rev.* 135 (2021) 110189.
[10] H. Tian, H. Jiao, J.M. Cai, J.W. Wang, Y. Yang, A.V. Bridgwater, Co-pyrolysis of *Miscanthus Sacchariflorus* and coals: A systematic study on the synergies in thermal decomposition, kinetics and vapour phase products, *Fuel* 262 (2020) 116603.
[11] R.M. Soncini, N.C. Means, N.T. Weiland, Co-pyrolysis of low rank coals and biomass: Product distributions, *Fuel* 112 (2013) 74–82.
[12] Z.Q. Wu, S.Z. Wang, J. Zhao, L. Chen, H.Y. Meng, Thermal behavior and char structure evolution of bituminous coal blends with edible fungi residue during co-pyrolysis, *Energy Fuels* 28 (3) (2014) 1792–1801.
[13] Y.Y. Song, A. Tahmasebi, J.L. Yu, Co-pyrolysis of pine sawdust and lignite in a thermogravimetric analyzer and a fixed-bed reactor, *Bioresour. Technol.* 174 (2014) 204–211.
[14] F.S. Yang, A.N. Zhou, W. Zhao, Z.Y. Yang, H.J. Li, Thermochemical behaviors, kinetics and gas emission analyses during co-pyrolysis of walnut shell and coal, *Thermochim. Acta* 673 (2019) 26–33.
[15] S.X. Qiu, S.F. Zhang, X.H. Zhou, Q.Y. Zhang, G.B. Qiu, M.L. Hu, Z.X. You, L.Y. Wen, C.G. Bai, Thermal behavior and organic functional structure of poplar-fat coal blends during co-pyrolysis, *Renew. Energy* 136 (2019) 308–316.
[16] A.O. Aboyade, J.F. Görgens, M. Carrier, E.L. Meyer, J.H. Knoetze, Thermogravimetric study of the pyrolysis characteristics and kinetics of coal blends with corn and sugarcane residues, *Fuel Process. Technol.* 106 (2013) 310–320.
[17] H.B. Vuthaluru, Thermal behaviour of coal/biomass blends during co-pyrolysis, *Fuel Process. Technol.* 85 (2–3) (2004) 141–155.
[18] A.K. Sadhukhan, P. Gupta, T. Goyal, R.K. Saha, Modelling of pyrolysis of coal-biomass blends using thermogravimetric analysis, *Bioresour. Technol.* 99 (17) (2008) 8022–8026.
[19] M.S. Masnadi, R. Habibi, J. Kopyscinski, J.M. Hill, X.T. Bi, C.J. Lim, N. Ellis, J.R. Grace, Fuel characterization and co-pyrolysis kinetics of biomass and fossil fuels, *Fuel* 117 (2014) 1204–1214.
[20] B.W. Lin, J.S. Zhou, Q.W. Qin, X. Song, Z.Y. Luo, Thermal behavior and gas evolution characteristics during co-pyrolysis of lignocellulosic biomass and coal: A TG-FTIR investigation, *J. Anal. Appl. Pyrolysis* 144 (2019) 104718.
[21] M. Ma, Y.H. Bai, X.D. Song, J.F. Wang, W.G. Su, M. Yao, G.S. Yu, Investigation into the co-pyrolysis behaviors of cow manure and coal blending by TG-MS, *Sci. Total. Environ.* 728 (2020) 138828.
[22] Z.Q. Wu, Y.W. Li, D.H. Xu, H.Y. Meng, Co-pyrolysis of lignocellulosic biomass with low-quality coal: Optimal design and synergistic effect from gaseous products distribution, *Fuel* 236 (2019) 43–54.
[23] S.D. Li, X.L. Chen, A.B. Liu, L. Wang, G.S. Yu, Study on co-pyrolysis characteristics of rice straw and Shenfu bituminous coal blends in a fixed bed reactor, *Bioresour. Technol.* 155 (2014) 252–257.
[24] S.J. Gerssen-Gondelach, D. Saygin, B. Wicke, M.K. Patel, A.P.C. Faaij, Competing uses of biomass: Assessment and comparison of the performance of bio-based heat, power, fuels and materials, *Renew. Sustain. Energy Rev.* 40 (2014) 964–998.
[25] K. Konwar, H.P. Nath, N. Bhuyan, B.K. Saikia, R.C. Borah, A.C. Kalita, N. Saikia, Effect of biomass addition on the devolatilization kinetics, mechanisms and thermodynamics of a northeast Indian low rank sub-bituminous coal, *Fuel* 256 (2019) 115926.
[26] S. Vyazovkin, C.A. Wight, Model-free and model-fitting approaches to kinetic analysis of isothermal and nonisothermal data, *Thermochim. Acta* 340–341 (1999) 53–68.
[27] Z.H. Chen, M. Hu, X.L. Zhu, D.B. Guo, S.M. Liu, Z.Q. Hu, B. Xiao, J.B. Wang, M. Laghari, Characteristics and kinetic study on pyrolysis of five lignocellulosic biomass *via* thermogravimetric analysis, *Bioresour. Technol.* 192 (2015) 441–450.
[28] E. Ranzi, A. Cuoci, T. Faravelli, A. Frassoldati, G. Migliavacca, S. Pierucci, S. Sommariva, Chemical kinetics of biomass pyrolysis, *Energy Fuels* 22 (6) (2008) 4292–4300.
[29] S. Sommariva, T. Maffei, G. Migliavacca, T. Faravelli, E. Ranzi, A predictive multi-step kinetic model of coal devolatilization, *Fuel* 89 (2) (2010) 318–328.
[30] T. Maffei, A. Frassoldati, A. Cuoci, E. Ranzi, T. Faravelli, Predictive one step kinetic model of coal pyrolysis for CFD applications, *Proc. Combust. Inst.* 34 (2) (2013) 2401–2410.
[31] D.M. Grant, R.J. Pugmire, T.H. Fletcher, A.R. Kerstein, Chemical model of coal devolatilization using percolation lattice statistics, *Energy Fuels* 3 (2) (1989) 175–186.
[32] A.D. Lewis, T.H. Fletcher, Prediction of sawdust pyrolysis yields from a flat-flame burner using the CPD model, *Energy Fuels* 27 (2) (2013) 942–953.
[33] A.K. Varma, P. Mondal, Physicochemical characterization and kinetic study of pine needle for pyrolysis process, *J. Therm. Anal. Calorim.* 124 (1) (2016) 487–497.
[34] A. Ashraf, H. Sattar, S. Munir, A comparative applicability study of model-fitting and model-free kinetic analysis approaches to non-isothermal pyrolysis of coal and agricultural residues, *Fuel* 240 (2019) 326–333.
[35] S. Saeed, M. Saleem, A. Durrani, Thermal performance analysis and synergistic effect on co-pyrolysis of coal and sugarcane bagasse blends pretreated by trihexyltetradecylphosphonium chloride, *Fuel* 278 (2020) 118240.
[36] A. Gupta, S.K. Thengane, S. Mahajani, Kinetics of pyrolysis and gasification of cotton stalk in the central parts of India, *Fuel* 263 (2020) 116752.
[37] A. Sahoo, S. Kumar, J. Kumar, T. Bhaskar, A detailed assessment of pyrolysis kinetics of invasive lignocellulosic biomasses (*Prosopis juliflora* and *Lantana camara*) by thermogravimetric analysis, *Bioresour. Technol.* 319 (2021) 124060.
[38] T. Ozawa, A new method of analyzing thermogravimetric data, *Bull. Chem. Soc. Jpn.* 38 (11) (1965) 1881–1886.
[39] C.X. Chen, X.Q. Ma, Y. He, Co-pyrolysis characteristics of microalgae *Chlorella vulgaris* and coal through TGA, *Bioresour. Technol.* 117 (2012) 264–273.

[40] Y.Y. He, C. Chang, P. Li, X.L. Han, H.L. Li, S.Q. Fang, J.Y. Chen, X.J. Ma, Thermal decomposition and kinetics of coal and fermented cornstalk using thermogravimetric analysis, *Bioresour. Technol.* 259 (2018) 294–303.
[41] L. Florentino-Madiedo, M.F. Vega, E. Díaz-Faes, C. Barriocanal, Evaluation of synergy during co-pyrolysis of torrefied sawdust, coal and paraffin, *A kinetic and thermodynamic dataset, Data Brief* 37 (2021) 107170.
[42] H.P. Nath, B.K. Dutta, D. Kalita, B.K. Saikia, N. Saikia, Evaluation of the effect of high sulfur subbituminous coal on the devolatilization of biomass residue by using model free, model fitting and combined kinetic methods, *Fuel* 310 (2022) 122235.
[43] A. Khawam, D.R. Flanagan, Complementary use of model-free and modelistic methods in the analysis of solid-state kinetics, *J. Phys. Chem. B* 109 (20) (2005) 10073–10080.
[44] R. Moriana, Y.J. Zhang, P. Mischnick, J.B. Li, M. Ek, Thermal degradation behavior and kinetic analysis of spruce glucomannan and its methylated derivatives, *Carbohydr. Polym.* 106 (2014) 60–70.
[45] S.R. Wang, H.Z. Lin, B. Ru, G.X. Dai, X.L. Wang, G. Xiao, Z.Y. Luo, Kinetic modeling of biomass components pyrolysis using a sequential and coupling method, *Fuel* 185 (2016) 763–771.
[46] H. Zhang, B.L. Dou, H. Zhang, J.J. Li, C.J. Ruan, C.F. Wu, Study on non-isothermal kinetics and the influence of calcium oxide on hydrogen production during bituminous coal pyrolysis, *J. Anal. Appl. Pyrolysis* 150 (2020) 104888.
[47] J.C. Yan, M.X. Liu, Z.H. Feng, Z.Q. Bai, H.F. Shui, Z.K. Li, Z.P. Lei, Z.C. Wang, S.B. Ren, S.G. Kang, H.L. Yan, Study on the pyrolysis kinetics of low-medium rank coals with distributed activation energy model, *Fuel* 261 (2020) 116359.
[48] É. de Godois Baroni, K. Tannous, Y.J. Rueda-Ordóñez, L.K. Tinoco-Navarro, The applicability of isoconversional models in estimating the kinetic parameters of biomass pyrolysis, *J. Therm. Anal. Calorim.* 123 (2) (2016) 909–917.
[49] J.H. Flynn, L.A. Wall, General treatment of the thermogravimetry of polymers, *J. Res. Natl. Bur. Stand. A Phys. Chem.* 70A (6) (1966) 487–523.
[50] H.E. Kissinger, Reaction kinetics in differential thermal analysis, *Anal. Chem.* 29 (11) (1957) 1702–1706.
[51] T. Akahira, T. Sunose, Method of determining activation deterioration constant of electrical insulating materials, *Res. Rep. Chiba Inst. Technol.* 16 (1971) 22–31.
[52] V. Bert, J. Allemon, P. Sajet, S. Dieu, A. Papin, S. Collet, R. Gaucher, M. Chalot, B. Michiels, C. Raventos, Torrefaction and pyrolysis of metal-enriched poplars from phytotechnologies: Effect of temperature and biomass chlorine content on metal distribution in end-products and valorization options, *Biomass Bioenergy* 96 (2017) 1–11.
[53] F. Rego, A.P. Soares Dias, M. Casquilho, F.C. Rosa, A. Rodrigues, Pyrolysis kinetics of short rotation coppice poplar biomass, *Energy* 207 (2020) 118191.
[54] Z.J. Cheng, X.Z. Gao, Z.H. Ma, X. Guo, J.L. Wang, P.P. Luan, S.R. He, B.B. Yan, G.Y. Chen, Studies on synergistic effects in co-pyrolysis of sargassum and poplar: Thermal behavior and kinetics, *J. Anal. Appl. Pyrolysis* 167 (2022) 105660.
[55] R. Lemaire, D. Menage, S. Menanteau, J.L. Harion, Experimental study and kinetic modeling of pulverized coal devolatilization under air and oxycombustion conditions at a high heating rate, *Fuel Process. Technol.* 128 (2014) 183–190.
[56] R. Lemaire, D. Menage, P. Seers, Study of the high heating rate devolatilization of bituminous and subbituminous coals—Comparison of experimentally monitored devolatilization profiles with predictions issued from single rate, two-competing rate, distributed activation energy and chemical percolation devolatilization models, *J. Anal. Appl. Pyrolysis* 123 (2017) 255–268.
[57] D. Menage, R. Lemaire, P. Seers, Experimental study and chemical reactor network modeling of the high heating rate devolatilization and oxidation of pulverized bituminous coals under air, oxygen-enriched combustion (OEC) and oxy-fuel combustion (OFC), *Fuel Process. Technol.* 177 (2018) 179–193.
[58] V. Balasundram, N. Ibrahim, R.M. Kasmani, M.K.A. Hamid, R. Isha, H. Hasbullah, R.R. Ali, Thermogravimetric catalytic pyrolysis and kinetic studies of coconut copra and rice husk for possible maximum production of pyrolysis oil, *J. Clean. Prod.* 167 (2017) 218–228.
[59] Y.F. Wu, J.L. Zhu, Y.M. Wang, H. Yang, L.J. Jin, H.Q. Hu, Insight into co-pyrolysis interactions of Pingshuo coal and high-density polyethylene *via in situ* Py-TOF-MS and EPR, *Fuel* 303 (2021) 121199.
[60] P.E. Sánchez-Jiménez, L.A. Pérez-Maqueda, A. Perejón, J.M. Criado, Generalized master plots as a straightforward approach for determining the kinetic model: The case of cellulose pyrolysis, *Thermochim. Acta* 552 (2013) 54–59.
[61] J.H. Flynn, The isoconversional method for determination of energy of activation at constant heating rates, *J. Therm. Anal.* 27 (1) (1983) 95–102.
[62] G.I. Senum, R.T. Yang, Rational approximations of the integral of the Arrhenius function, *J. Therm. Anal.* 11 (3) (1977) 445–447.
[63] J. Wang, S.Y. Zhang, X. Guo, A.X. Dong, C. Chen, S.W. Xiong, Y.T. Fang, W.D. Yin, Thermal behaviors and kinetics of Pingshuo coal/biomass blends during copyrolysis and cocombustion, *Energy Fuels* 26 (12) (2012) 7120–7126.
[64] A. Blazej, M. Kosik, Phytomass: A Raw Material for Chemistry and Biotechnology, Ellis Horwood, New York, 1993.
[65] E. Kastanaki, D. Vamvuka, P. Grammelis, E. Kakaras, Thermogravimetric studies of the behavior of lignite-biomass blends during devolatilization, *Fuel Process. Technol.* 77–78 (2002) 159–166.
[66] H. Wu, H. Li, Z. Zhao, Thermogravimetric analysis and pyrolytic kinetic study on coal/biomass blends, *J. Fuel Chem. Technol.* 37 (2009) 538–545.
[67] H.Y. Zhao, Q. Song, S.C. Liu, Y.H. Li, X.H. Wang, X.Q. Shu, Study on catalytic co-pyrolysis of physical mixture/staged pyrolysis characteristics of lignite and straw over an catalytic beds of char and its mechanism, *Energy Convers. Manag.* 161 (2018) 13–26.
[68] Y. Zhao, L. Liu, P.H. Qiu, X. Xie, X.Y. Chen, D. Lin, S.Z. Sun, Impacts of chemical fractionation on Zhundong coal's chemical structure and pyrolysis reactivity, *Fuel Process. Technol.* 155 (2017) 144–152.
[69] T.B. Gu, Z.F. Fu, T. Berning, X.T. Li, C.G. Yin, A simplified kinetic model based on a universal description for solid fuels pyrolysis: Theoretical derivation, experimental validation, and application demonstration, *Energy* 225 (2021) 120133.
[70] B. Tian, X.R. Wang, W.Y. Zhao, L. Xu, L. Bai, Pyrolysis behaviors, kinetics and gaseous product evolutions of two typical biomass wastes, *Catal. Today* 374 (2021) 77–85.
[71] S. Vyazovkin, K. Chrissafis, M.L. di Lorenzo, N. Koga, M. Pijolat, B. Roduit, N. Sbirrazzuoli, J.J. Suñol, ICTAC Kinetics Committee recommendations for collecting experimental thermal analysis data for kinetic computations, *Thermochim. Acta* 590 (2014) 1–23.
[72] F. Nardella, M. Mattonai, E. Ribechini, Evolved gas analysis-mass spectrometry and isoconversional methods for the estimation of component-specific kinetic data in wood pyrolysis, *J. Anal. Appl. Pyrolysis* 145 (2020) 104725.
[73] K. Slopiecka, P. Bartocci, F. Fantozzi, Thermogravimetric analysis and kinetic study of poplar wood pyrolysis, *Appl. Energy* 97 (2012) 491–497.
[74] J.C. Yan, H.R. Jiao, Z.K. Li, Z.P. Lei, Z.C. Wang, S.B. Ren, H.F. Shui, S.G. Kang, H.L. Yan, C.X. Pan, Kinetic analysis and modeling of coal pyrolysis with model-free methods, *Fuel* 241 (2019) 382–391.
[75] F. Ferrara, A. Orsini, A. Plaisant, A. Pettinau, Pyrolysis of coal, biomass and their blends: Performance assessment by thermogravimetric analysis, *Bioresour. Technol.* 171 (2014) 433–441.
[76] A.C. Minh Loy, S. Yusup, B.L. Fui Chin, D.K. Wai Gan, M. Shahbaz, M.N. Acda, P. Unrean, E. Rianawati, Comparative study of *in situ* catalytic pyrolysis of rice husk for syngas production: Kinetics modelling and product gas analysis, *J. Clean. Prod.* 197 (2018) 1231–1243.
[77] D.K.W. Gan, A.C.M. Loy, B.L.F. Chin, S. Yusup, P. Unrean, E. Rianawati, M.N. Acda, Kinetics and thermodynamic analysis in one-pot pyrolysis of rice hull using renewable calcium oxide based catalysts, *Bioresour. Technol.* 265 (2018) 180–190.
[78] R.K. Mishra, K. Mohanty, Pyrolysis kinetics and thermal behavior of waste sawdust biomass using thermogravimetric analysis, *Bioresour. Technol.* 251 (2018) 63–74.
[79] Y.M. Ding, O.A. Ezekoye, S.X. Lu, C.J. Wang, R. Zhou, Comparative pyrolysis behaviors and reaction mechanisms of hardwood and softwood, *Energy Convers. Manag.* 132 (2017) 102–109.
[80] R.K. Singh, T. Patil, D. Pandey, S.P. Tekade, A.N. Sawarkar, Co-pyrolysis of petroleum coke and banana leaves biomass: Kinetics, reaction mechanism, and thermodynamic analysis, *J. Environ. Manag.* 301 (2022) 113854.
[81] Q. He, C. Cheng, X.S. Zhang, Q.H. Guo, L. Ding, A. Raheem, G.S. Yu, Insight into structural evolution and detailed non-isothermal kinetic analysis for coal pyrolysis, *Energy* 244 (2022) 123101.
[82] Y.H. Li, H.Y. Zhao, X. Sui, X.M. Wang, H.B. Ji, Studies on individual pyrolysis and co-pyrolysis of peat-biomass blends: Thermal decomposition behavior, possible synergism, product characteristic evaluations and kinetics, *Fuel* 310 (2022) 122280.
[83] Q.R. Liu, H.Q. Hu, Q. Zhou, S.W. Zhu, G.H. Chen, Effect of inorganic matter on reactivity and kinetics of coal pyrolysis, *Fuel* 83 (6) (2004) 713–718.
[84] M. Sharifzadeh, M. Sadeqzadeh, M. Guo, T.N. Borhani, N.V.S.N. Murthy Konda, M.C. Garcia, L. Wang, J. Hallett, N. Shah, The multi-scale challenges of biomass fast pyrolysis and bio-oil upgrading: Review of the state of art and future research directions, *Prog. Energy Combust. Sci.* 71 (2019) 1–80.
[85] X. Hu, M. Gholizadeh, Biomass pyrolysis: A review of the process development and challenges from initial researches up to the commercialisation stage, *J. Energy Chem.* 39 (2019) 109–143.
[86] G. Mishra, T. Bhaskar, Non isothermal model free kinetics for pyrolysis of rice straw, *Bioresour. Technol.* 169 (2014) 614–621.
[87] S. Sobek, S. Werle, Solar pyrolysis of waste biomass: A comparative study of products distribution, *in situ* heating behavior, and application of model-free kinetic predictions, *Fuel* 292 (2021) 120365.
[88] W. Wang, R. Lemaire, Global kinetic modeling of the devolatilization of pulverized coal and poplar wood in a thermogravimetric analyzer and a flat flame reactor, in: Proceedings of the Combustion Institute – Canadian Section, Spring Technical Meeting, The University of Ottawa, Canada, 2022.